Polar Geosci., **17**, 57–87, 2004

High-grade metamorphic rocks from Skallevikshalsen in the Lützow-Holm Complex, East Antarctica: Metamorphic conditions and possibility of partial melting

Yasutaka Yoshimura[1*], Yoichi Motoyoshi[2], Tomoharu Miyamoto[3], Edward S. Grew[4], Christopher J. Carson[5†] and Daniel J. Dunkley[2]

[1] *Department of Natural Environmental Science, Kochi University, Akebono-cho 2-chome, Kochi 780-8520*
[2] *National Institute of Polar Research, Kaga 1-chome, Itabashi-ku, Tokyo 173-8515*
[3] *Department of Earth and Planetary Sciences, Kyushu University, Hakozaki 6-chome, Fukuoka 812-8581*
[4] *Department of Geological Science, University of Maine, 5790 Bryand Research Center, Orono, Maine 04469-5790, U.S.A.*
[5] *Geologcal Survey of Canada, 601 Booth St., Ottowa, Canada K1A0E8*
[†] *now at Northern Territory Geological Survey, GOP 3000, Darwin NT, 0801, Australia*
[*] *Corresponding author. E-mail: yosimura@cc.kochi-u.ac.jp*

(Received April 30, 2004; Accepted August 9, 2004)

Abstract: The high-grade metamorphic rocks of Skallevikshalsen, Lützow-Holm Complex, East Antarctica predominantly comprise garnet-sillimanite gneiss, garnet-spinel-sillimanite gneiss, garnet-biotite gneiss and garnet-two pyroxene-mafic granulite. The metamorphic conditions were estimated using various geothermometers and geobarometers for garnet-biotite gneiss and mafic gneiss. The results were 770–940℃ and 0.65–1.2 GPa for garnet-biotite gneiss and 780–960℃ and 0.6–1.1 GPa for mafic gneiss.

Garnet-biotite gneiss is widespread in this area and displays a well-developed migmatitic structure. Garnet porphyroblasts in the leucosome and the boundaries between leucosome and melanosome in garnet-biotite gneiss commonly have a poikiloblastic texture with euhedral feldspar and quartz inclusions. High Y concentrations in garnet cores, high An values for plagioclase inclusions, and high Ba contents in K-feldspar from garnet-biotite gneiss are inferred to reflect growth in the presence of partial melt. Garnet in garnet-sillimanite gneiss also has high Y and P contents and chemical zoning that implies changes in trace element distribution coefficients. It is suggested that hydrous melt in garnet-sillimanite gneiss was generated during prograde metamorphism while anhydrous restite underwent continuous high-temperature metamorphism. Garnet-sillimanite gneiss is likely to be the restitic product of partial melting and shows evidence for melt segregation and movement.

key words: high-grade metamorphic rocks, mineral chemistry, partial melting, Skallevikshalsen, Lützow-Holm Complex

1. Introduction

High-grade metamorphic rocks are the dominant components of the lower crust, and the process of their formation and modification is important in understanding the tectonics and the evolution of continental crust. Futhermore, high-temperature meta-

morphism is commonly accompanied by partial melting, which is an important process for the generation of granite magma within continental crust.

Upper amphibolite to granulite facies metamorphic rocks in the Lützow-Holm Complex are exposed along the Prince Olav Coast and Lützow-Holm Bay, East Antarctica. Metamorphism, inferred from U-Pb SHRIMP data to have occurred between *ca*. 520–550 Ma (Shiraishi *et al*., 1992, 1994), is characterized by a clockwise *P-T* path, as indicated by the presence of prograde kyanite and staurolite inclusions within garnet or plagioclase and the development of reaction textures characteristic of near-isothermal decompression (Hiroi *et al*., 1983, 1986; Motoyoshi, 1986; Motoyoshi and Ishikawa, 1997; Fraser *et al*., 2000). Recent research results estimate the peak metamorphic conditions in the Lützow-Holm Complex during this event at over 1000°C (Motoyoshi and Ishikawa, 1997; Yoshimura *et al*., in prep.). Under such high-temperature conditions, it is probable that high grade metamorphism was accompanied by partial melting. Therefore, this complex is important not only in the study of the Pan-African orogeny and tectonothermal event, but in modeling the development and evolution of continental crust.

This paper describes garnet-bearing high-grade metamorphic rocks from Skallevikshalsen, and estimates the peak metamorphic conditions. In addition, the possibility of partial melting is discussed based on the texture of garnet and the chemical composition of minerals.

2. Geological setting

The Lützow-Holm Complex shows a marked westward progression in metamorphic grade from upper amphibolite facies to granulite facies. The thermal axis is presumed to be around Rundvågshetta in the southern part of Lützow-Holm Bay (Motoyoshi, 1986).

Skallevikshalsen is located in the south-western part of the Lützow-Holm Complex within the granulite-facies zone, about 70 km southwest of Syowa Station and about 30 km northeast of Rundvågshetta (Fig. 1). According to Yoshida *et al*. (1976), orthogneiss (brown gneissose granodiorite and garnet gneissose granite), paragneiss and marble associated with skarn are widely distributed in this region. Minor amount of metabasite are also present as lenses and layers within orthogneiss and paragneiss (Fig. 2).

Field studies in Skallevikshalsen carried out by JARE-40 (Japanese Antarctic Research Expedition, 1998–1999 season) indicate that the region consists of orthopyroxene felsic gneiss, garnet-sillimanite, garnet-biotite gneiss and crystalline limestone, with subordinate garnet-spinel-sillimanite gneiss and mafic gneiss. Orthopyroxene felsic gneiss is the most common lithology and was designated as brown gneissose granodiorite by Yoshida *et al*. (1976) and orthopyroxene gneiss by Shiraishi *et al*. (1989). Garnet-sillimanite gneiss, garnet-biotite gneiss and garnet-spinel-sillimanite gneiss belong to the paragneiss category of Yoshida *et al*. (1976) and layered pelitic gneiss is described by Shiraishi *et al*. (1989). Mafic gneiss corresponds to metabasite of Yoshida *et al*. (1976). This paper describes garnet-sillimanite gneiss, garnet-spinel-sillimanite gneiss, garnet-biotite gneiss and mafic gneiss. The sampling sites for EPMA analysis are shown in Fig. 2 and the samples are described in detail in the next chapter.

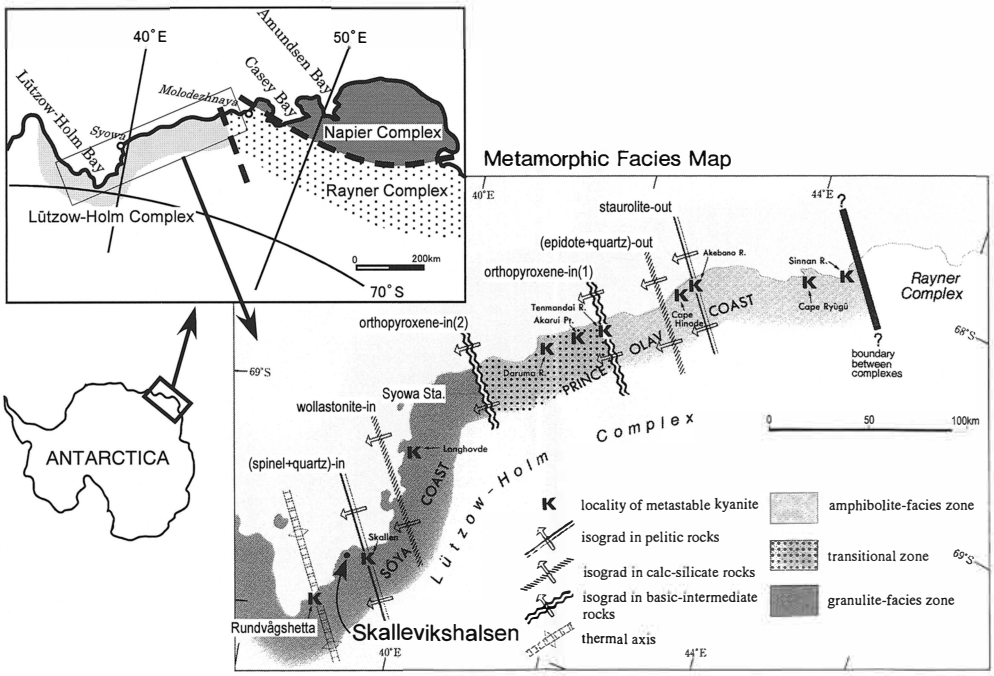

Fig. 1. Location of Skallevikshalsen and metamorphic facies map for the Lützow-Holm Complex. Metamorphic facies are after Shiraishi et al. (1989).

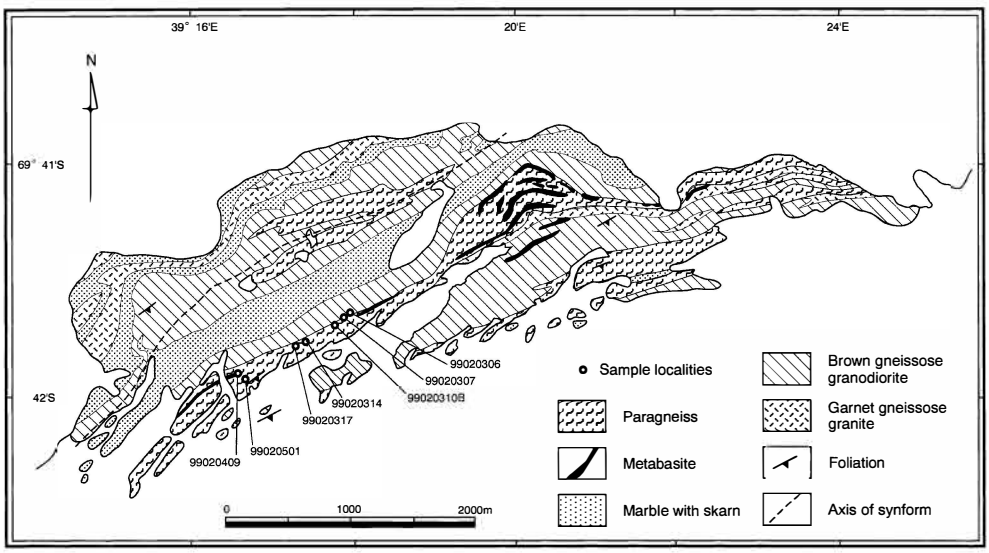

Fig. 2. Simplified geological map of Skallevikshalsen (after Yoshida et al., 1976; Matsueda et al., 1983), showing localities of samples used for chemical analysis in this study. Garnet-sillimanite gneiss, garnet-spinel-sillimanite gneiss and garnet-biotite gneiss belong to the paragneiss category of lithology indicated in the map. Mafic gneiss corresponds to metabasite.

3. Petrography

3.1. Garnet-sillimanite gneiss

Garnet-sillimanite gneiss is present in the central and southern parts of this area. Field occurrence, photographs of polished surfaces and thin-section photographs of rock samples are shown in Fig. 3. Garnet-sillimanite gneiss is divided into two main types, based on garnet grain size: coarse-grained (about 2–3 cm diameter) garnet-bearing type (Fig. 3a) and fine-grained (where garnet grains are about 5 mm or smaller) garnet-bearing type (Fig. 3b). Figure 3c and d show polished surface and thin-section photographs depicting the representative mineral assemblages in fine-grained garnet-bearing type. The rocks contain garnet, sillimanite, plagioclase, K-feldspar, quartz and graphite. Hydrous minerals are markedly absent. The fine-grained garnet-bearing type is moderately well foliated, and garnet and sillimanite grains are aligned parallel to the gneissic fabric. The core portions of garnet grains contain numerous fine-grained inclusions (Fig. 3d). Some inclusions are euhedral to subhedral quartz and feldspar. Since the coarse-grained garnet-bearing lithology has undergone intense weathering, we chose the fine-grained garnet-bearing type for detailed observation of thin sections and for EPMA analysis.

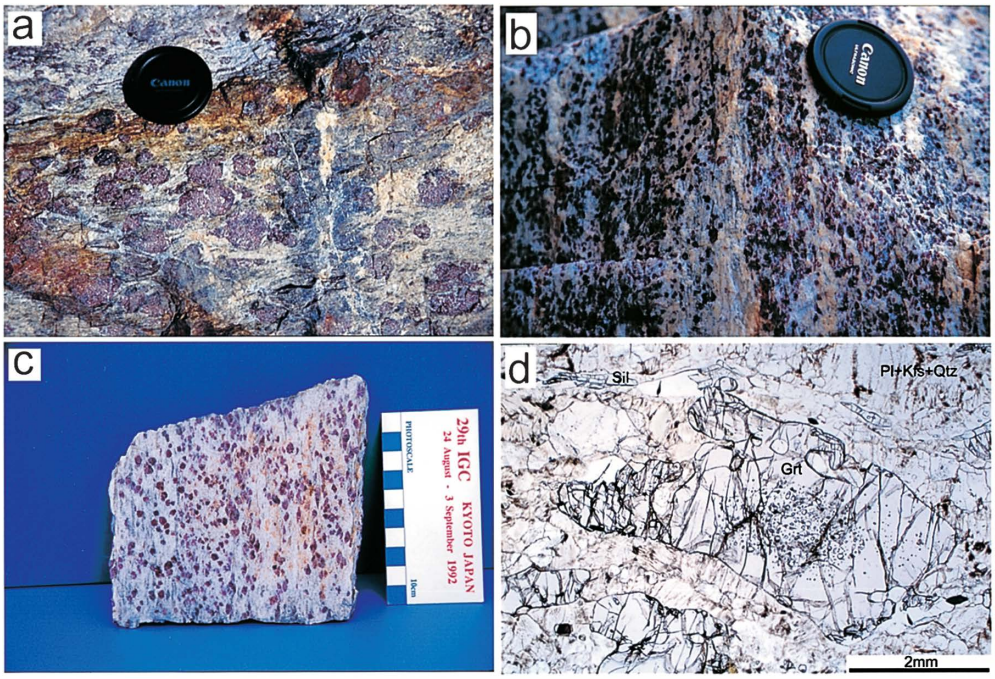

Fig. 3. (a) and (b) Outcrop photographs, (c) polished surface photograph, and (d) photomicrograph of garnet-sillimanite gneiss from Skallevikshalsen. (a) Coarse-grained garnet-bearing type. (b) Fine-grained garnet-bearing type. (c) Polished surface of fine-grained garnet-bearing type. (d) Garnet with numerous fine-grained inclusions (Sample No. 99020310B). Plane polarized light. Grt: garnet, Sil: sillimanite, Pl: plagioclase, Kfs: K-feldspar, Qtz: quartz.

3.2. Garnet-spinel-sillimanite gneiss

Garnet-spinel-sillimanite gneiss is intercalated with garnet-sillimanite gneiss. This rock type commonly exhibits gneissose layering (Fig. 4a), although locally this structure is poorly defined (Fig. 4b). Photomicrographs of typical thin-sections are shown in Fig. 5. The gneiss is rich in coarsely crystalline garnet, spinel, sillimanite, corundum, plagioclase, K-feldspar and quartz, and contains a small amount of biotite. Spinel and corundum are not found in association with quartz. This rock has aggregates of symplectitic spinel and plagioclase surrounding coarse-grained garnet and sillimanite (Fig. 5a and c). Spinel and plagioclase symplectitic aggregates are aligned parallel to the gneissic fabric. Spinel is dark-green to opaque under plane-polarized light. Columnar crystals of corundum occur in spinel-rich domains (Fig. 5b–e), and are locally associated with sillimanite (Fig. 5d). Biotite is rarely present in domains that are rich in spinel and plagioclase (Fig. 5e). There are no symplectitic coronas surrounding garnet grains. Spinel and plagioclase symplectitic aggregates are aligned parallel to the gneissic fabric (Fig. 5f).

3.3. Garnet-biotite gneiss

Garnet-biotite gneiss is widespread in this area and displays a well-developed gneissosity. The rock contains well-developed leucosomes of various sizes that are concordant with, semi-concordant with, or discordant to the dominant gneissic fabric

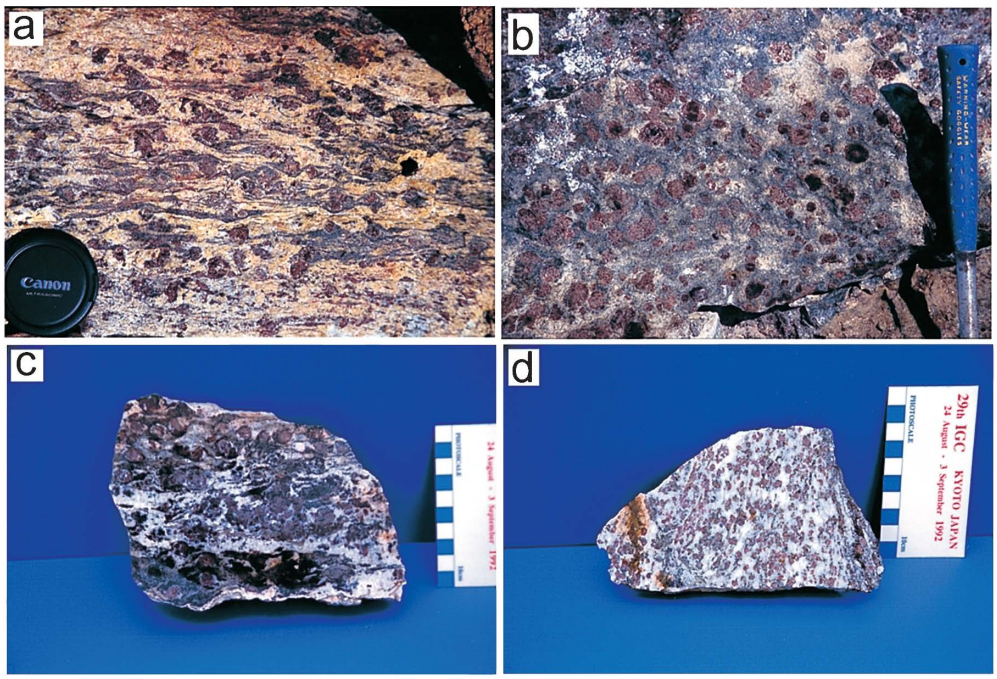

Fig. 4. (a) and (b) Outcrop photographs, and (c), (d) polished surface photographs of garnet-spinel-sillimanite gneiss. (c) Sample No. 99020317. (d) Sample No. 99020307.

(Fig. 6). Garnet-biotite gneiss can be subdivided, based on the sizes of garnet grain and modal abundance of biotite, into melanocratic and leucocratic types. Stromatic and schlieren leucosome is developed in both types. Both types consist predominantly of garnet, biotite, plagioclase, K-feldspar and quartz, with minor sillimanite. Photomicrographs of typical garnet-biotite gneiss are shown in Fig. 7. The melanocratic type has coarse-grained garnet (about 3–6 mm diameter) and a higher modal abundance of

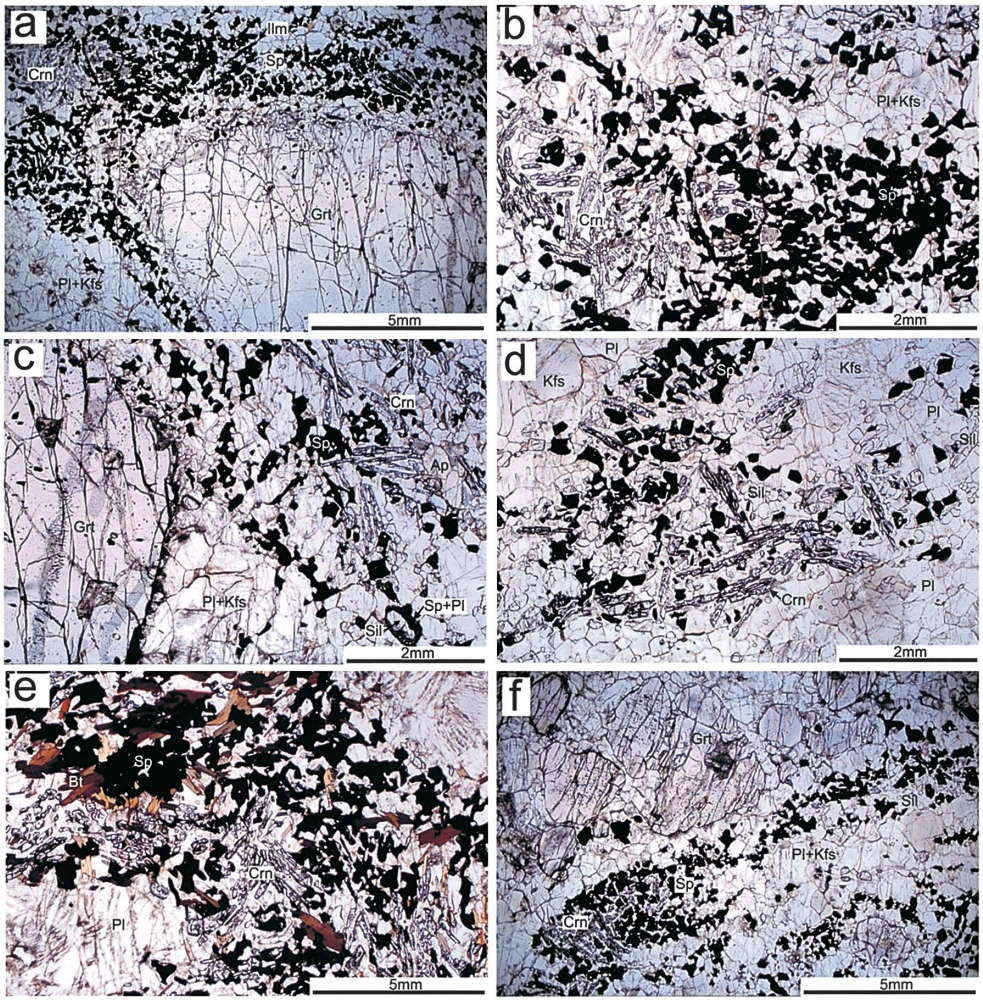

Fig. 5. Photomicrographs of garnet-spinel-sillimanite gneiss from Skallevikshalsen. Plane polarized light. (a) Aggregates of symplectitic spinel and plagioclase surrounding coarse-grained garnet (Sample: 99020317). (b) Columnar crystals of corundum in spinel-rich domain (Sample: 99020317). (c) Symplectitic spinel and plagioclase surrounding sillimanite (Sample: 99020317). (d) Corundum associated with sillimanite, spinel and plagioclase (Sample: 99020317). (e) Biotite in spinel and corundum-rich domain (Sample: 99020314). (f) Spinel-plagioclase symplectitic aggregates aligned parallel to the gneissic fabric (Sample: 99020307). Sp: spinel, Crn: corundum, Ilm: ilmenite, Bt: biotite.

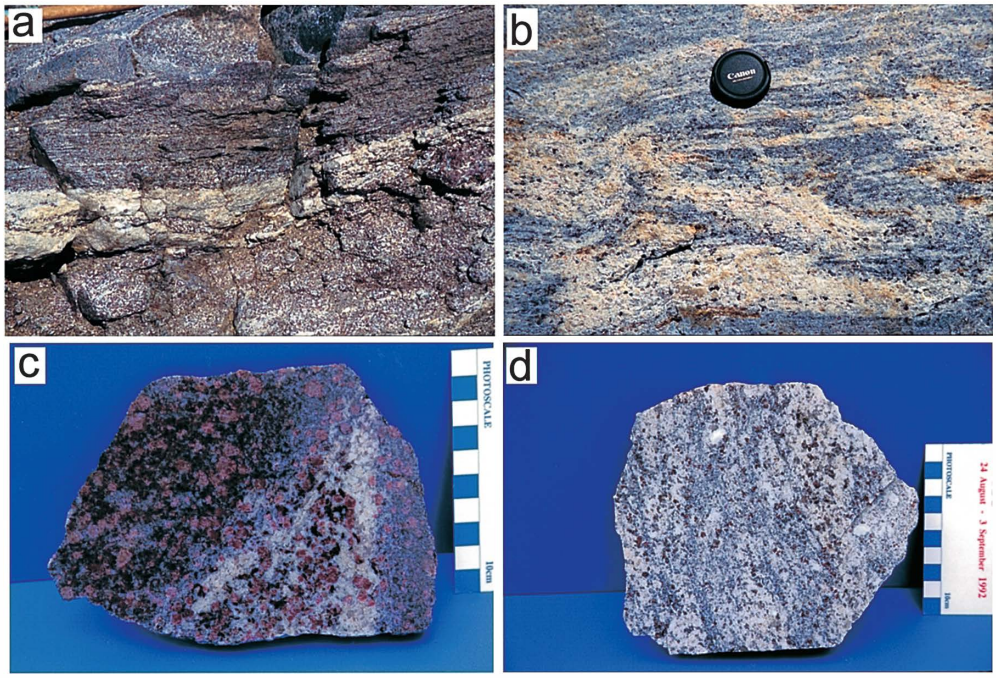

Fig. 6. (a) and (b) Outcrop photographs, and (c) and (d) polished surface photographs of garnet-biotite gneiss. (a) and (c) Melanocratic type (Sample No. 99020306), (b) and (d) leucocratic type (Sample No. 99020501).

biotite than the leucocratic type. These garnet crystals usually contain dusty cores and clear, almost inclusion-free margins. The dusty appearance in the core is due to the presence of abundant inclusions. In the melanosome of the melanocratic type, garnet grains are anhedral and show irregular morphologies with dusty cores (Fig. 7a). These garnet grains are lack clear margins near concave edges. In contrast, coarse-grained garnet porphyroblasts in the leucosome and the boundary part between leucosome and melanosome commonly have idioblastic to subidioblastic and poikiloblastic textures with euhedral feldspar and quartz inclusions, and almost complete clear rims (Fig. 7b and c). In the leucocratic rock type, garnet grains are idioblastic to subidioblastic and lack dusty cores (Fig. 7e). Apatite is a common constituent mineral and is relatively coarse-grained (about 0.2–0.4 mm in size) in the leucocratic type. The leucosomes have more coarse-grained feldspar and quartz than melanosomes in both rock types (Fig. 7d and f).

3.4. Mafic gneiss (garnet-two pyroxene-amphibole gneiss)

Mafic gneiss is present as blocks or lenticular masses within garnet-biotite gneiss, garnet-sillimanite geniss and orthopyroxene felsic gneiss, where it is either massive or gneissic in structure (Fig. 8a). Figures 8b–d show characteristic thin-section views of mafic gneiss. The dominant minerals are garnet, orthopyroxene, clinopyroxene, amphibole, plagioclase, and quartz, with minor amounts of biotite. Garnet, pyroxene and amphibole are moderately to coarsely crystalline (about 2–5 mm) and have sub-

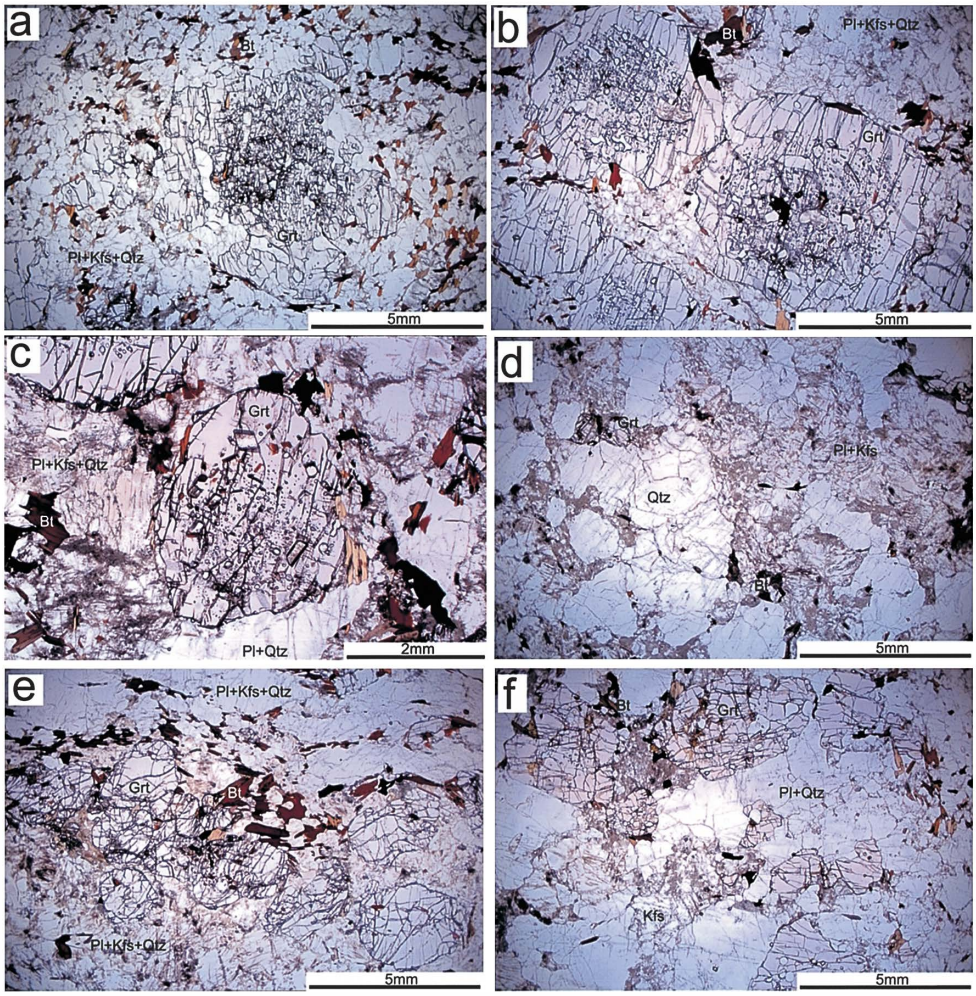

Fig. 7. Photomicrographs of garnet-biotite gneiss. Plane polarized light. (a) Melanosome in melanocratic type (Sample: 99020306-M), (b) boundary between melanosome and leucosome in melanocratic type (Sample: 99020306-B), (c) and (d) leucosome in melanocratic type (Sample: 99020306-L), (e) and (f) leucocratic type of garnet-biotite gneiss (Sample: 99020501).

idioblastic to xenoblastic textures. Pyroxene grains and amphibole are elongate parallel to the gneissic fabric.

4. Chemical composition of metamorphic minerals

4.1. Analytical techniques

A list of mineral assemblages of studied samples of garnet-sillimanite gneiss, garnet-spinel-sillimanite gneiss, garnet-biotite gneiss and mafic gneiss is presented in Table 1. Constituent minerals were analyzed with EPMA, and the results for garnet,

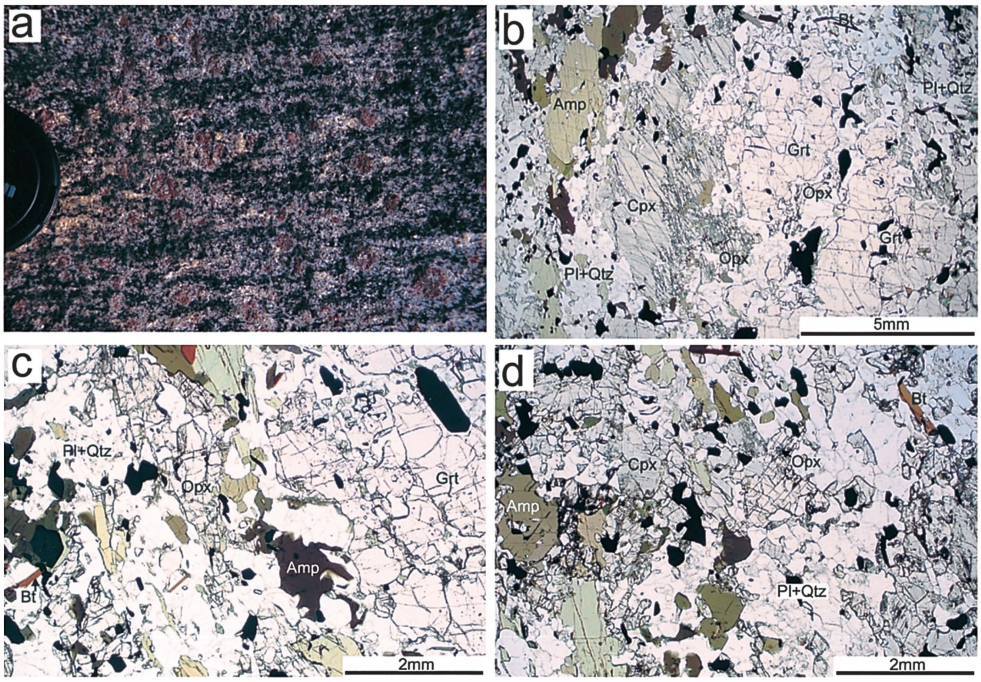

Fig. 8. (a) Outcrop photograph and (b), (c) and (d) photomicrographs of mafic gneiss (garnet-two pyroxene-hornblende gneiss). Sample: 99020409. Opx: orthopyroxene, Cpx: clinopyroxene, Amp: amphibole.

Table 1. Mineral assemblages of analyzed samples from Skallevikshalsen.

Sample No.	Grt	Bt	Opx	Cpx	Amp	Sil	Sp	Crn	Pl	Kfs	Qtz
Grt-Sil gneiss											
99020310B	++					+			++	+	+
Grt-Sp-Sil gneiss											
99020307	++					+	++		++	+	+
99020314	++	+				+	++	+	++	+	
99020317	++					+	++	+	++	+	+
Grt-Bt gneiss											
melanocratic type											
99020306-M	++	++				+			++	+	+
99020306-L	++	++							++	++	++
99020306-B	++	++							++	++	++
leucocratic type											
99020501	++	+				+			++	++	++
Mafic gneiss											
99020409	++	+	++	++	++				++		+

++: abundant, +medium

Mineral abbreviations: Grt: garnet, Bt: biotite, Opx: orthopyroxene, Cpx: clinopyroxene, Amp: amphibole, Sil: sillimanite, Sp: spinel, Crn: corundum, Pl: plagioclase, Kfs: K-feldspar, Qtz: quartz.

Table 2. Representative electron microprobe analyses of minerals from Skallevikshalsen.

mineral	Garnet (O=12)																		
rock type	Grt-Sil gneiss			Grt-Sp-Sil gneiss			Grt-Bt gneiss: melanocratic type								leuccocratic type		Mafic gneiss:		
sample No.	99020310B			99020307	99010317		99020306-M			99020306-L		99020306-B			99020501		99020409		
SiO_2	39.25	39.10	39.37	37.80	38.19	38.11	39.55	39.62	39.81	39.67	39.29	38.96	39.34	39.61	38.06	38.07	38.21	37.85	38.37
TiO_2	0.04	0.02	0.02	0.07	0.01	0.09	0.01	0.02	0.03	0.03	0.04	0.00	0.07	0.03	0.03	0.01	0.05	0.07	0.05
Al_2O_3	21.94	22.12	22.17	21.12	21.48	21.43	22.05	22.08	22.09	22.13	22.10	21.99	22.25	22.04	21.32	21.53	21.50	21.28	21.58
Y_2O_3	0.08	0.03	0.00	0.03	0.03	0.00	0.00	0.06	0.01	0.00	0.09	0.00	0.03	0.05	0.12	0.10	0.02	0.03	0.00
Yb_2O_3	0.01	0.00	0.01	0.00	0.00	0.00	0.00	0.00	0.02	0.02	0.00	0.00	0.00	0.01	0.05	0.00	0.00	0.00	0.00
Cr_2O_3	0.05	0.00	0.05	0.01	0.02	0.01	0.02	0.00	0.03	0.08	0.01	0.09	0.08	0.00	0.00	0.00	0.01	0.00	0.01
FeO*	27.50	27.55	27.61	31.89	33.04	31.23	25.45	25.09	25.60	26.79	26.13	27.39	25.45	26.06	31.52	31.96	28.47	28.36	28.35
MnO	0.67	0.66	0.63	0.59	0.56	0.36	0.65	0.58	0.54	0.57	0.49	0.64	0.58	0.53	0.74	0.79	0.88	0.87	0.76
NiO	0.00	0.00	0.00	0.00	0.00	0.00	0.00	0.00	0.00	0.00	0.00	0.00	0.00	0.00	0.00	0.00	0.00	0.00	0.00
MgO	9.42	9.35	9.82	3.16	5.62	4.06	10.21	10.57	10.89	10.35	9.70	9.55	9.57	10.38	4.60	5.13	3.72	3.56	3.99
CaO	1.69	1.80	1.06	5.80	1.64	5.39	2.31	2.20	1.58	1.31	2.51	1.41	3.17	2.03	4.01	2.73	8.11	8.05	7.96
Na_2O	0.01	0.00	0.01	0.00	0.00	0.00	0.00	0.01	0.00	0.00	0.00	0.00	0.00	0.00	0.01	0.01	0.01	0.00	0.01
K_2O	0.00	0.00	0.00	0.00	0.00	0.00	0.00	0.00	0.00	0.00	0.00	0.00	0.00	0.00	0.00	0.00	0.00	0.00	0.00
P_2O_5	0.07	0.02	0.12	0.06	0.01	0.02	0.05	0.01	0.04	0.07	0.02	0.09	0.00	0.02	0.04	0.00	0.01	0.00	0.00
Total	100.74	100.65	100.86	100.53	100.60	100.69	100.30	100.23	100.63	101.02	100.38	100.11	100.54	100.74	100.50	100.35	100.98	100.06	101.06
Si	2.999	2.991	2.996	2.998	3.001	2.999	3.009	3.010	3.011	3.004	2.999	2.991	2.994	3.005	3.001	3.000	2.990	2.992	2.994
Ti	0.002	0.001	0.001	0.004	0.001	0.005	0.001	0.001	0.002	0.001	0.002	0.000	0.004	0.001	0.002	0.001	0.003	0.004	0.003
Al	1.975	1.994	1.989	1.974	1.990	1.987	1.977	1.977	1.969	1.975	1.988	1.990	1.996	1.971	1.982	1.999	1.983	1.982	1.984
Y	0.003	0.001	0.000	0.001	0.001	0.000	0.000	0.002	0.000	0.000	0.004	0.000	0.001	0.002	0.005	0.004	0.001	0.001	0.000
Yb	0.000	0.000	0.000	0.000	0.000	0.000	0.000	0.000	0.000	0.001	0.000	0.000	0.000	0.000	0.001	0.000	0.000	0.000	0.000
Cr	0.003	0.000	0.003	0.001	0.001	0.001	0.001	0.000	0.002	0.005	0.001	0.005	0.005	0.000	0.000	0.000	0.000	0.000	0.001
Fe^{2+}	1.757	1.762	1.757	2.115	2.171	2.055	1.619	1.594	1.619	1.696	1.667	1.759	1.620	1.653	2.078	2.106	1.863	1.875	1.850
Mn	0.044	0.043	0.041	0.040	0.037	0.024	0.042	0.037	0.034	0.037	0.031	0.042	0.037	0.034	0.050	0.053	0.058	0.058	0.050
Ni	0.000	0.000	0.000	0.000	0.000	0.000	0.000	0.000	0.000	0.000	0.000	0.000	0.000	0.000	0.000	0.000	0.000	0.000	0.000
Mg	1.073	1.067	1.114	0.374	0.658	0.476	1.157	1.197	1.228	1.169	1.103	1.093	1.086	1.173	0.540	0.603	0.434	0.419	0.464
Ca	0.139	0.148	0.087	0.493	0.138	0.454	0.189	0.179	0.128	0.107	0.205	0.116	0.259	0.165	0.338	0.231	0.680	0.682	0.665
Na	0.002	0.000	0.001	0.000	0.000	0.000	0.001	0.002	0.000	0.000	0.000	0.000	0.000	0.000	0.002	0.002	0.001	0.000	0.001
K	0.000	0.000	0.000	0.000	0.000	0.000	0.000	0.000	0.000	0.000	0.000	0.000	0.000	0.000	0.000	0.000	0.000	0.000	0.000
P	0.004	0.001	0.007	0.004	0.001	0.001	0.003	0.000	0.003	0.005	0.001	0.006	0.000	0.001	0.002	0.000	0.001	0.000	0.000
Total	8.002	8.008	7.996	8.004	8.001	8.001	7.998	8.000	7.997	7.998	8.001	8.002	8.001	8.006	8.001	7.998	8.014	8.013	8.011
X_{Mg}	0.38	0.38	0.39	0.15	0.23	0.19	0.42	0.43	0.43	0.41	0.40	0.38	0.40	0.42	0.21	0.22	0.19	0.18	0.20
Pyr	35.63	35.33	37.14	12.36	21.91	15.82	38.49	39.80	40.81	38.85	36.68	36.33	36.18	38.78	17.97	20.15	14.31	13.81	15.32
Alm	58.32	58.37	58.61	70.02	72.26	68.29	53.84	53.00	53.80	56.39	55.45	58.44	53.96	54.64	69.12	70.37	61.38	61.80	61.07
Sps	1.45	1.41	1.36	1.31	1.24	0.80	1.39	1.25	1.14	1.22	1.05	1.39	1.24	1.13	1.65	1.77	1.93	1.92	1.65
Grs	4.60	4.89	2.89	16.31	4.60	15.09	6.27	5.95	4.25	3.54	6.83	3.85	8.62	5.46	11.25	7.71	22.39	22.48	21.96

* = Total Fe as FeO

Table 2. (Continued).

mineral	Biotite (O=22)														
rock type	Grt-Sp-Sil gneiss				Grt-Bt gneiss										
					melanocratic type									leucocratic type		
sample No.	99020314				99020306-M			99020306-L			99020306-B			99020501		
SiO_2	36.93	35.90	35.83	35.92	39.21	38.34	37.94	37.24	38.42	38.15	37.49	36.98	38.62	36.93	35.82	36.73
TiO_2	5.35	5.20	5.89	5.04	6.01	5.78	6.13	6.00	6.25	6.97	5.93	6.35	6.04	4.19	4.30	4.46
Al_2O_3	17.80	17.55	17.56	17.76	15.39	15.78	15.73	16.00	16.04	16.02	15.51	15.79	15.52	16.25	16.26	15.78
Cr_2O_3	0.00	0.07	0.05	0.00	0.04	0.09	0.03	0.19	0.14	0.06	0.14	0.22	0.03	0.04	0.03	0.01
FeO*	15.44	14.61	15.54	16.59	8.44	11.20	11.31	12.30	13.08	9.59	11.26	11.96	9.17	17.87	16.90	18.34
MnO	0.00	0.03	0.00	0.01	0.03	0.00	0.03	0.03	0.02	0.03	0.01	0.04	0.00	0.01	0.01	0.00
NiO	0.00	0.00	0.00	0.00	0.00	0.00	0.00	0.00	0.00	0.00	0.00	0.00	0.00	0.00	0.00	0.00
MgO	12.10	11.88	11.97	11.79	16.10	15.11	14.93	14.74	14.41	15.91	15.13	14.59	17.55	11.67	10.97	11.10
CaO	0.00	0.00	0.34	0.00	0.00	0.00	0.00	0.00	0.01	0.00	0.00	0.01	0.00	0.01	0.02	0.00
Na_2O	0.14	0.10	0.08	0.13	0.03	0.05	0.05	0.05	0.02	0.32	0.01	0.01	0.16	0.12	0.06	0.09
K_2O	10.13	10.39	10.36	10.56	9.97	10.58	10.33	10.21	9.76	9.90	10.77	10.57	9.24	10.42	10.04	10.00
P_2O_5	0.02	0.03	0.01	0.01	0.02	0.02	0.00	0.01	0.03	0.01	0.01	0.01	0.02	0.01	0.00	0.01
ZnO	0.07	0.00	0.00	0.06	0.04	0.10	0.23	0.02	0.18	0.17	0.21	0.25	0.21	0.04	0.03	0.01
BaO	0.00	0.00	0.00	0.00	0.00	0.00	0.00	0.00	0.00	0.00	0.00	0.00	0.00	0.00	0.00	0.00
F	0.58	0.34	0.32	0.18	1.26	0.89	1.01	0.71	0.68	0.86	1.55	1.43	1.35	1.20	1.21	1.52
O=	-0.25	-0.14	-0.14	-0.08	-0.53	-0.37	-0.42	-0.30	-0.29	-0.36	-0.65	-0.60	-0.57	-0.50	-0.51	-0.64
Total	98.31	95.95	97.82	97.96	95.99	97.57	97.29	97.20	98.73	97.63	97.37	97.61	97.34	98.26	95.14	97.41
Si	5.380	5.355	5.271	5.297	5.666	5.542	5.509	5.430	5.502	5.460	5.479	5.408	5.522	5.485	5.476	5.518
Ti	0.586	0.583	0.651	0.559	0.653	0.629	0.670	0.658	0.673	0.751	0.652	0.698	0.650	0.468	0.495	0.504
Al	3.056	3.086	3.046	3.086	2.621	2.689	2.693	2.749	2.707	2.703	2.671	2.721	2.615	2.845	2.930	2.793
Cr	0.000	0.009	0.006	0.000	0.004	0.011	0.003	0.022	0.016	0.007	0.016	0.025	0.003	0.005	0.003	0.001
Fe^{2+}	1.881	1.823	1.912	2.046	1.020	1.354	1.374	1.500	1.566	1.148	1.376	1.463	1.097	2.219	2.161	2.304
Mn	0.000	0.004	0.000	0.001	0.003	0.000	0.004	0.003	0.002	0.004	0.001	0.005	0.000	0.002	0.001	0.000
Ni	0.000	0.000	0.000	0.000	0.000	0.000	0.000	0.000	0.000	0.000	0.000	0.000	0.000	0.000	0.000	0.000
Mg	2.627	2.641	2.624	2.592	3.469	3.256	3.233	3.203	3.076	3.394	3.296	3.180	3.740	2.584	2.501	2.486
Ca	0.000	0.000	0.053	0.000	0.000	0.000	0.000	0.000	0.002	0.000	0.000	0.002	0.000	0.001	0.003	0.000
Na	0.040	0.028	0.023	0.036	0.010	0.015	0.013	0.015	0.006	0.087	0.003	0.004	0.043	0.034	0.018	0.027
K	1.883	1.977	1.945	1.986	1.837	1.951	1.913	1.900	1.783	1.808	2.009	1.973	1.686	1.975	1.958	1.917
P	0.002	0.004	0.001	0.001	0.002	0.002	0.000	0.001	0.004	0.001	0.002	0.001	0.003	0.002	0.000	0.001
Zn	0.008	0.000	0.000	0.006	0.004	0.011	0.024	0.002	0.019	0.018	0.023	0.027	0.022	0.004	0.003	0.001
Ba	0.000	0.000	0.000	0.000	0.000	0.000	0.000	0.000	0.000	0.000	0.000	0.000	0.000	0.000	0.000	0.000
Total	15.464	15.511	15.533	15.611	15.290	15.459	15.436	15.483	15.354	15.380	15.529	15.507	15.380	15.624	15.551	15.551
X_{Mg}	0.58	0.59	0.58	0.56	0.77	0.71	0.70	0.68	0.66	0.75	0.71	0.68	0.77	0.54	0.54	0.52

* = Total Fe as FeO

Table 2. (Continued).

mineral	Plagioclase (O=8)																	
rock type	Grt-Sil gneiss		Grt-Sp-Sil gneiss										leucocratic type		Mafic gneiss			
sample No.	99020310B		99020307		99020314	99020317		99020306-M		99020306-L		99020306-B		99020501	99020409			
SiO_2	60.43	60.40	61.38	53.34	60.77	58.56	53.31	56.65	57.21	56.71	59.16	55.47	58.42	60.18	60.00	47.36	48.31	49.86
TiO_2	0.00	0.02	0.02	0.00	0.00	0.01	0.02	0.00	0.02	0.00	0.03	0.00	0.03	0.00	0.01	0.00	0.02	0.01
Al_2O_3	25.05	24.95	23.99	29.58	24.03	25.84	29.24	26.96	26.92	26.74	25.22	27.97	25.71	24.83	24.99	33.25	32.72	31.52
Cr_2O_3	0.00	0.00	0.04	0.03	0.02	0.00	0.03	0.00	0.00	0.01	0.00	0.00	0.00	0.03	0.00	0.00	0.00	0.00
FeO*	0.01	0.00	0.05	0.02	0.21	0.42	0.23	0.00	0.01	0.49	0.00	0.12	0.04	0.00	0.03	0.12	0.08	0.17
MnO	0.00	0.01	0.00	0.00	0.00	0.01	0.03	0.00	0.00	0.00	0.05	0.00	0.02	0.00	0.03	0.10	0.00	0.00
NiO	0.00	0.00	0.00	0.00	0.00	0.00	0.00	0.00	0.00	0.00	0.00	0.00	0.00	0.00	0.00	0.00	0.00	0.00
MgO	0.00	0.00	0.01	0.02	0.00	0.01	0.02	0.00	0.00	0.01	0.00	0.00	0.00	0.00	0.00	0.00	0.00	0.01
CaO	6.65	6.41	5.54	12.32	5.18	7.60	11.83	9.02	8.58	8.86	7.19	10.39	8.00	6.67	6.24	16.89	16.01	15.01
Na_2O	7.69	7.72	8.22	4.48	8.15	6.96	4.53	6.03	6.36	5.96	7.27	5.46	6.91	7.79	7.70	1.73	2.19	2.94
K_2O	0.29	0.47	0.33	0.16	0.44	0.41	0.22	0.56	0.45	0.66	0.28	0.34	0.33	0.25	0.33	0.04	0.04	0.12
P_2O_5	0.08	0.05	0.19	0.02	0.12	0.07	0.06	0.03	0.10	0.01	0.08	0.00	0.09	0.04	0.03	0.01	0.04	0.03
BaO	0.00	0.00	0.00	0.00	0.00	0.00	0.00	0.02	0.00	0.03	0.01	0.00	0.00	0.00	0.00	0.00	0.00	0.00
Total	100.20	100.04	99.75	99.96	98.93	99.89	99.52	99.26	99.64	99.46	99.30	99.76	99.53	99.78	99.34	99.51	99.40	99.67
Si	2.685	2.689	2.731	2.415	2.728	2.625	2.424	2.562	2.573	2.566	2.657	2.505	2.625	2.686	2.687	2.184	2.222	2.284
Ti	0.000	0.001	0.001	0.000	0.000	0.000	0.001	0.000	0.001	0.000	0.001	0.000	0.001	0.000	0.000	0.000	0.001	0.000
Al	1.311	1.309	1.258	1.578	1.272	1.365	1.567	1.437	1.427	1.426	1.335	1.489	1.361	1.306	1.319	1.807	1.774	1.701
Cr	0.000	0.000	0.001	0.001	0.001	0.000	0.001	0.000	0.000	0.000	0.000	0.000	0.000	0.001	0.000	0.000	0.000	0.000
Fe^{2+}	0.000	0.000	0.002	0.001	0.008	0.016	0.009	0.000	0.000	0.019	0.000	0.005	0.002	0.000	0.001	0.005	0.003	0.006
Mn	0.000	0.000	0.000	0.000	0.000	0.000	0.001	0.000	0.000	0.000	0.002	0.000	0.001	0.000	0.001	0.004	0.000	0.000
Ni	0.000	0.000	0.000	0.000	0.000	0.000	0.000	0.000	0.000	0.000	0.000	0.000	0.000	0.000	0.000	0.000	0.000	0.000
Mg	0.000	0.000	0.000	0.001	0.000	0.000	0.001	0.000	0.000	0.000	0.000	0.000	0.000	0.000	0.000	0.000	0.000	0.000
Ca	0.316	0.306	0.264	0.598	0.249	0.365	0.576	0.437	0.413	0.430	0.346	0.503	0.385	0.319	0.299	0.834	0.789	0.737
Na	0.663	0.667	0.709	0.393	0.710	0.605	0.399	0.529	0.555	0.522	0.633	0.478	0.602	0.674	0.668	0.155	0.195	0.261
K	0.017	0.027	0.019	0.009	0.025	0.023	0.013	0.032	0.026	0.038	0.016	0.019	0.019	0.014	0.019	0.002	0.003	0.007
P	0.003	0.002	0.007	0.001	0.005	0.003	0.002	0.001	0.004	0.000	0.003	0.000	0.003	0.001	0.001	0.000	0.001	0.001
Ba	0.000	0.000	0.000	0.000	0.000	0.000	0.000	0.000	0.000	0.000	0.000	0.000	0.000	0.000	0.000	0.000	0.000	0.000
Total	4.995	5.000	4.992	4.996	4.997	5.002	4.994	4.999	4.998	5.001	4.994	4.999	4.999	5.002	4.995	4.991	4.987	4.998
Ca/(Ca+Na)	0.32	0.31	0.27	0.60	0.26	0.38	0.59	0.45	0.43	0.45	0.35	0.51	0.39	0.32	0.31	0.84	0.80	0.74
Ab	66.56	66.70	71.47	39.31	72.13	60.92	40.39	52.99	55.81	52.78	63.59	47.77	59.82	66.93	67.76	15.62	19.76	25.95
An	31.77	30.61	26.62	59.78	25.31	36.72	58.34	43.77	41.60	43.40	34.78	50.28	38.29	31.67	30.35	84.15	79.98	73.34
Or	1.67	2.69	1.91	0.91	2.57	2.36	1.27	3.23	2.59	3.82	1.63	1.94	1.89	1.41	1.89	0.22	0.26	0.71

* = Total Fe as FeO

Table 2. (Continued).

mineral	K-feldspar (O=8)								mineral	Orthopyroxene (O=6)			Clinopyroxene (O=6)		Amphibole (O=23)		Spinel (O=4)	
rock type	Grt-Sil gneiss		Grt-Sp-Sil gneiss		Grt-Bt gneiss				rock type	Mafic gneiss			Mafic gneiss		Mafic gneiss		Grt-Sp-Sil gneiss	
					melanocratic type		leucocratic type											
sample No.	99020310B		99020314		99020306-L		99020501		sample No.	99020409			99020409		99020409		99020317	
SiO_2	64.80	64.90	64.87	65.49	64.89	64.56	64.81	64.81	SiO_2	50.17	50.25	50.12	50.04	50.44	41.76	41.11	0.00	0.00
TiO_2	0.04	0.06	0.03	0.03	0.08	0.11	0.00	0.03	TiO_2	0.11	0.08	0.07	0.28	0.34	1.98	2.37	0.04	0.03
Al_2O_3	18.04	17.86	17.97	18.74	18.01	18.36	18.07	18.11	Al_2O_3	0.64	0.69	0.62	1.79	2.30	12.25	11.66	58.92	59.41
Cr_2O_3	0.00	0.00	0.00	0.00	0.01	0.01	0.02	0.03	Cr_2O_3	0.03	0.02	0.02	0.00	0.02	0.00	0.01	0.09	0.09
FeO*	0.03	0.00	0.04	0.00	0.00	0.00	0.04	0.01	FeO*	35.30	34.58	34.32	22.70	19.57	18.13	19.58	35.70	34.10
MnO	0.00	0.00	0.00	0.00	0.01	0.03	0.03	0.01	MnO	0.51	0.58	0.59	0.38	0.36	0.12	0.16	0.08	0.11
NiO	0.00	0.00	0.00	0.00	0.00	0.00	0.00	0.00	NiO	0.00	0.00	0.00	0.00	0.00	0.00	0.00	0.01	0.03
MgO	0.00	0.01	0.00	0.01	0.00	0.00	0.00	0.01	MgO	13.18	13.49	13.36	10.37	10.76	8.37	7.82	5.39	5.42
CaO	0.07	0.14	0.08	0.20	0.09	0.12	0.06	0.06	CaO	0.82	0.77	0.74	14.60	16.51	11.55	11.31	0.00	0.00
Na_2O	0.97	1.26	1.15	3.12	0.90	1.17	1.22	1.15	Na_2O	0.00	0.00	0.00	0.19	0.23	1.24	1.25	0.00	0.00
K_2O	15.77	15.24	15.49	12.18	15.71	15.11	15.34	15.42	K_2O	0.00	0.00	0.00	0.00	0.00	1.83	1.77	0.00	0.00
P_2O_5	0.07	0.08	0.09	0.09	0.05	0.07	0.03	0.04	P_2O_5	0.00	0.00	0.01	0.00	0.00	0.06	0.00	0.02	0.02
ZnO	-	-	-	-	-	-	-	-	ZnO	-	-	-	-	-	-	-	0.14	0.08
BaO	0.45	0.40	0.23	0.31	0.77	0.57	0.42	0.30	BaO	-	-	-	-	-	0.00	0.00	-	-
F	-	-	-	-	-	-	-	-	F	-	-	-	-	-	0.00	0.00	-	-
O=	-	-	-	-	-	-	-	-	O=	-	-	-	-	-	0.00	0.00	-	-
Total	100.24	99.95	99.95	100.16	100.53	100.11	100.04	99.98	Total	100.76	100.45	99.86	100.36	100.54	97.29	97.04	100.38	99.30
Si	2.997	3.003	3.001	2.986	2.998	2.985	2.998	2.998	Si	1.979	1.981	1.986	1.946	1.939	6.371	6.345	0.000	0.000
Ti	0.002	0.002	0.001	0.001	0.003	0.004	0.000	0.001	Ti	0.003	0.002	0.002	0.008	0.010	0.228	0.275	0.001	0.001
Al	0.983	0.974	0.980	1.007	0.981	1.001	0.985	0.987	Al	0.030	0.032	0.029	0.082	0.104	2.202	2.121	1.950	1.972
Cr	0.000	0.000	0.000	0.000	0.001	0.000	0.001	0.001	Cr	0.001	0.001	0.001	0.000	0.001	0.000	0.001	0.002	0.002
Fe^{2+}	0.001	0.000	0.001	0.000	0.000	0.000	0.002	0.000	Fe^{2+}	1.164	1.140	1.137	0.738	0.629	2.312	2.527	0.839	0.803
Mn	0.000	0.000	0.000	0.000	0.000	0.001	0.001	0.000	Mn	0.017	0.019	0.020	0.012	0.012	0.016	0.020	0.002	0.003
Ni	0.000	0.000	0.000	0.000	0.000	0.000	0.000	0.000	Ni	0.000	0.000	0.000	0.000	0.000	0.000	0.000	0.000	0.001
Mg	0.000	0.001	0.000	0.000	0.000	0.000	0.000	0.001	Mg	0.775	0.792	0.789	0.601	0.616	1.903	1.799	0.226	0.228
Ca	0.003	0.007	0.004	0.010	0.005	0.006	0.003	0.003	Ca	0.035	0.032	0.032	0.608	0.680	1.889	1.870	0.000	0.000
Na	0.087	0.113	0.103	0.276	0.080	0.105	0.110	0.103	Na	0.000	0.000	0.000	0.015	0.017	0.366	0.373	0.000	0.000
K	0.931	0.899	0.914	0.708	0.926	0.891	0.905	0.910	K	0.000	0.000	0.000	0.000	0.000	0.355	0.348	0.000	0.000
P	0.003	0.003	0.003	0.004	0.002	0.003	0.001	0.002	P	0.000	0.000	0.000	0.000	0.000	0.008	0.000	0.000	0.001
Zn	-	-	-	-	-	-	-	-	Zn	-	-	-	-	-	-	-	0.003	0.002
Ba	0.008	0.007	0.004	0.006	0.014	0.010	0.008	0.006	Ba	-	-	-	-	-	0.000	0.000	-	-
Total	5.015	5.010	5.012	4.997	5.009	5.005	5.014	5.011	Total	4.003	4.000	3.996	4.012	4.007	15.649	15.680	3.022	3.011
Ca/(Ca+Na)	0.04	0.06	0.04	0.03	0.05	0.05	0.03	0.03	X_{Mg}	0.40	0.41	0.41	0.45	0.49	0.45	0.42	0.21	0.22
Ab	8.54	11.09	10.10	27.74	7.94	10.44	10.76	10.12	En	39.25	40.33	40.30	30.87	32.02	-	-	-	-
An	0.32	0.69	0.41	0.97	0.45	0.59	0.30	0.31	Fs	59.00	58.02	58.09	37.90	32.67	-	-	-	-
Or	91.13	88.22	89.50	71.29	91.61	88.98	88.94	89.57	Wo	1.75	1.64	1.61	31.23	35.31	-	-	-	-

* = Total Fe as FeO - = not determined

biotite, plagioclase, K-feldspar, orthopyroxene, clinopyroxene and amphibole are given in Table 2. The analyses were performed using a wave-length dispersive (WDS) electron probe microanalyzer (JEOL JXA-8600MX) installed at Kochi University. For quantitative analyses, an acceleration voltage of 15 kV, probe current of 1.5×10^{-8} A, and beam diameter of 1 or 5 μm were used. X-ray intensity data were reduced using an oxide-ZAF correction. For compositional mapping, an acceleration voltage of 15 kV, probe current of 7.5×10^{-7}A, dwell time of 50 ms and beam diameter of 5 μm were used.

4.2. Mineral compositions

4.2.1. Garnet

Garnet from all the rock types is essentially a pyrope (Prp)-almandine (Alm)-grossular (Grs) solid solution with low spessartine(Sps) components. Variations in garnet compositions are shown in a partial Mg-Fe-Ca ternary diagram (Fig. 9). Garnet core compositions from garnet-sillimanite gneiss, garnet-spinel-sillimanite gneiss, melanocratic garnet-biotite gneiss, leucocratic garnet-biotite gneiss and mafic gneiss are $Prp_{33-35}Alm_{58-60}Sps_{1-2}Grs_{4-5}$, $Prp_{12-16}Alm_{68-72}Sps_{1-2}Grs_{15-17}$, $Prp_{35-37}Alm_{55-56}Sps_{1-2}Grs_{6-9}$, $Prp_{16-18}Alm_{68-70}Sps_{1-2}Grs_{11-12}$ and $Prp_{13-14}Alm_{61-62}Sps_{1-2}Grs_{22-23}$, respectively. Pyrope contents of garnets in garnet-sillimanite gneiss and melanocratic garnet-biotite gneiss are higher than other rock types. Compositions of the most Mg-rich portions of garnet from garnet-sillimanite gneiss, garnet-spinel-sillimanite gneiss, garnet-biotite gneiss and mafic gneiss are $Prp_{35-38}Alm_{58-60}Sps_{1-2}Grs_{3-4}$, $Prp_{17-23}Alm_{71-78}Sps_{1-2}Grs_{4-7}$, $Prp_{37-41}Alm_{53-56}Sps_{1-2}Grs_{4-6}$, $Prp_{17-18}Alm_{68-69}Sps_{1-2}Grs_{8-10}$ and $Prp_{15-16}Alm_{60-61}Sps_{1-2}Grs_{21-22}$, respectively.

The X_{Mg}-P_2O_5 plot and X_{Mg}-Y_2O_3 [where $X_{Mg}=Mg/(Mg+Fe)$] plot for garnet are shown in Fig.10 and Fig. 11. The P_2O_5 content in garnet is highest garnet-sillimanite gneiss, up to 0.12 wt%. Garnet-spinel-sillimanite gneiss and garnet-biotite gneiss con-

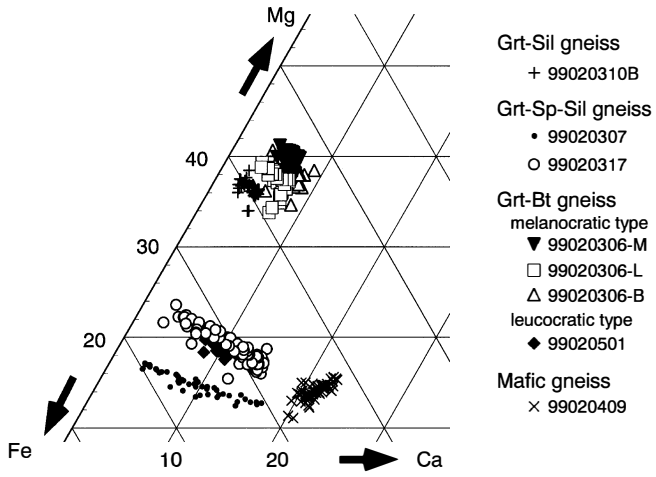

Fig. 9. Mg-Fe-Ca ratio of garnet compositions. 99020306-M: melanosome of melanocratic type. 99020306-L: leucosome of melanocratic type. 99020306-B: boundary between melanosome and leucosome of melanocratic type.

tain up to 0.06–0.08 wt% P_2O_5. Garnet in leucocratic garnet-biotite gneiss has the highest Y_2O_3 content, up to 0.13 wt%. The Y content of garnet in garnet-sillimanite gneiss and melanocratic garnet-biotite gneiss is up to 0.1 wt%.

Typical color X-ray intensity maps for garnet are shown in Figs. 12–16. Garnet porphyroblasts from Skallevikshalsen show clear compositional zoning, with CaO

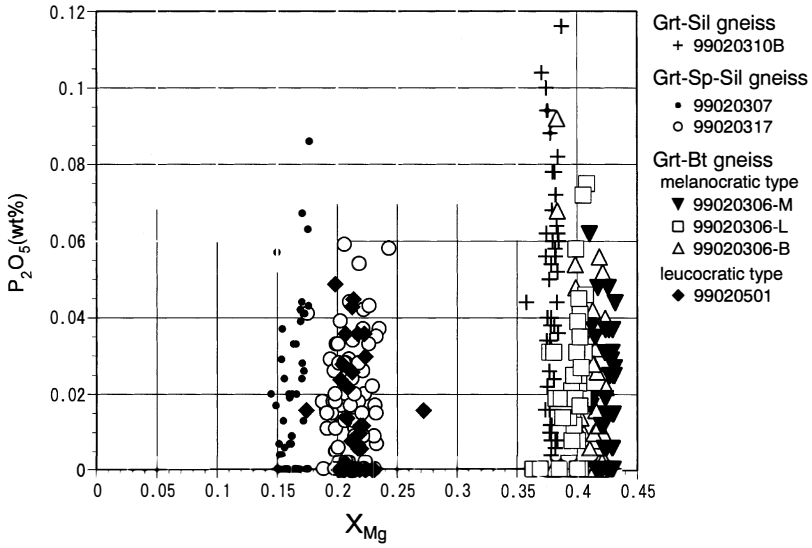

Fig. 10. Variation of P_2O_5 and X_{Mg} of garnet. 99020306-M: melanosome of melanocratic type. 99020306-L: leucosome of melanocratic type. 99020306-B: boundary part between melanosome and leucosome of melanocratic type.

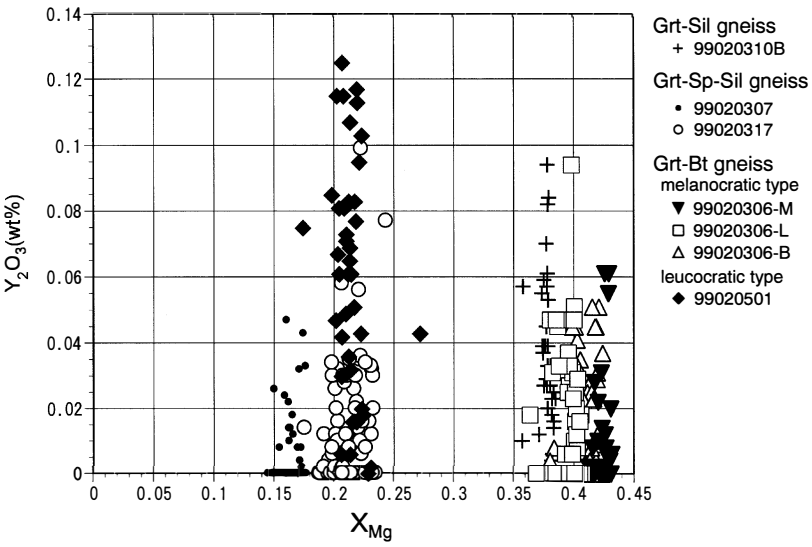

Fig. 11. Variation of Y_2O_3 and X_{Mg} in garnet.

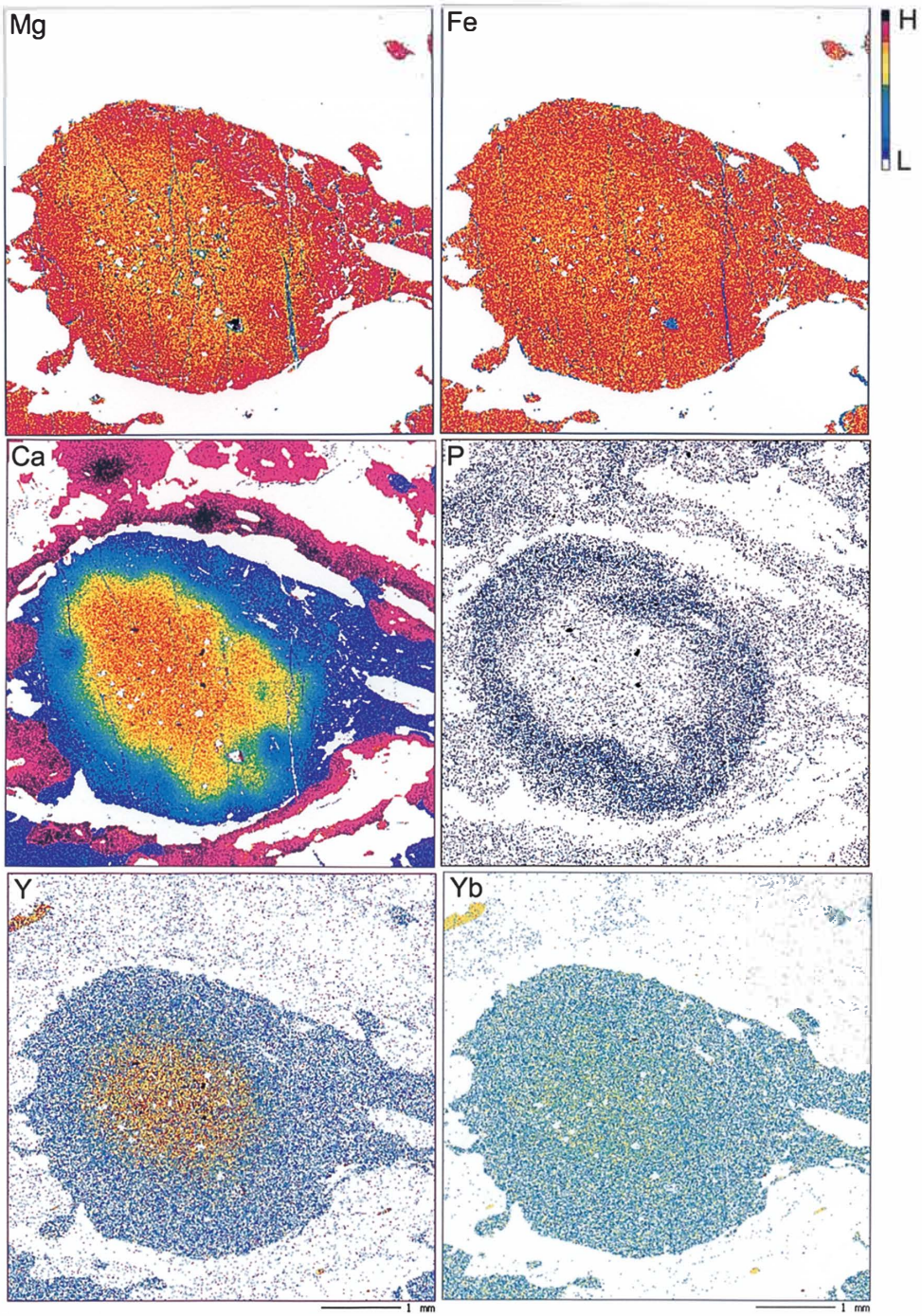

Fig. 12. Color X-ray intensity map of garnet in garnet-sillimanite gneiss (Sample: 99020310B). H and L represent higher and lower X-ray count intensity which reflects higher and lower concentrations of each element, respectively.

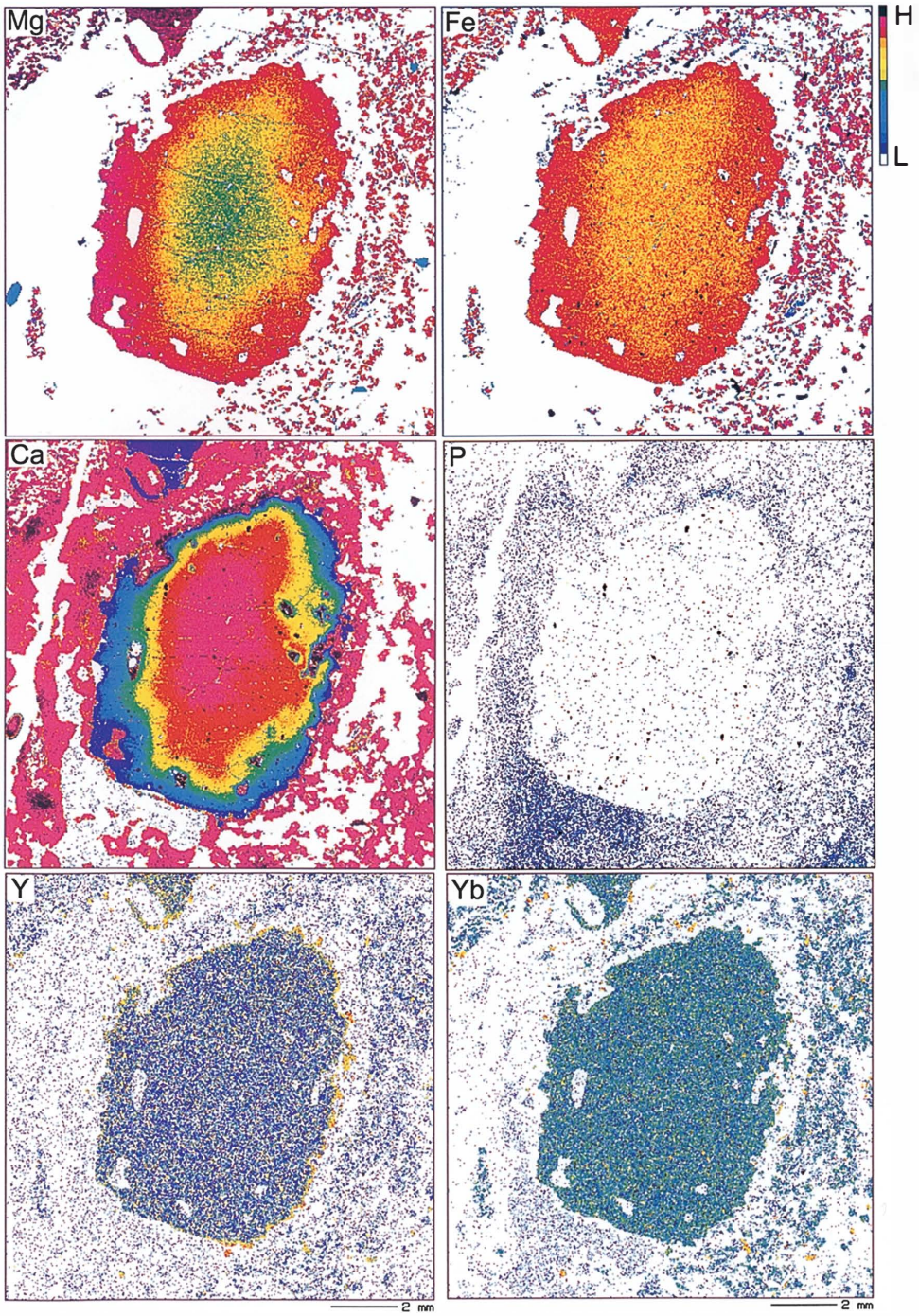

Fig. 13. Color X-ray intensity map of garnet in garnet-spinel-sillimanite gneiss (Sample: 99020317).

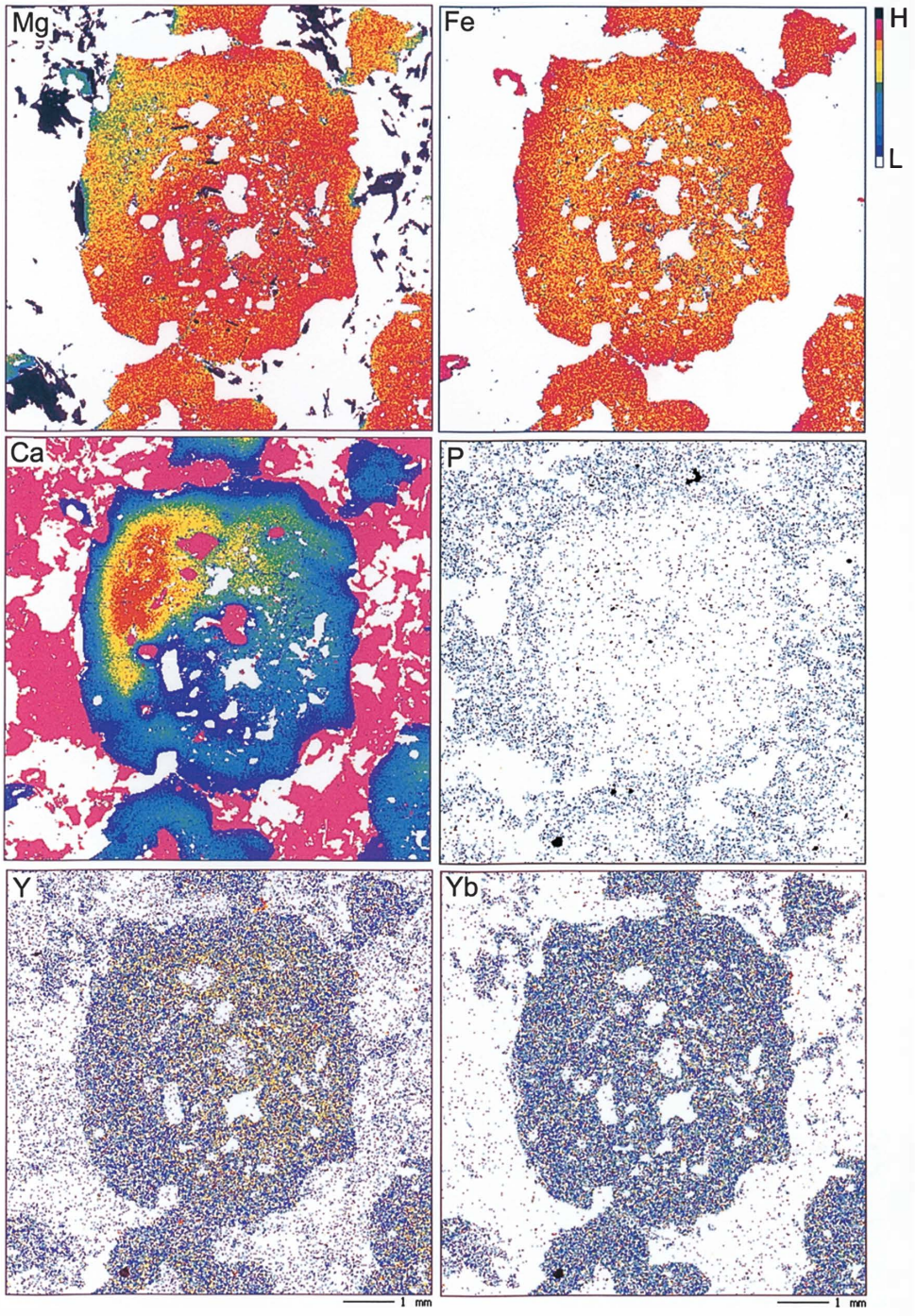

Fig. 14. Color X-ray intensity map of garnet in melanocratic garnet-biotite gneiss (Sample: 99020306-B).

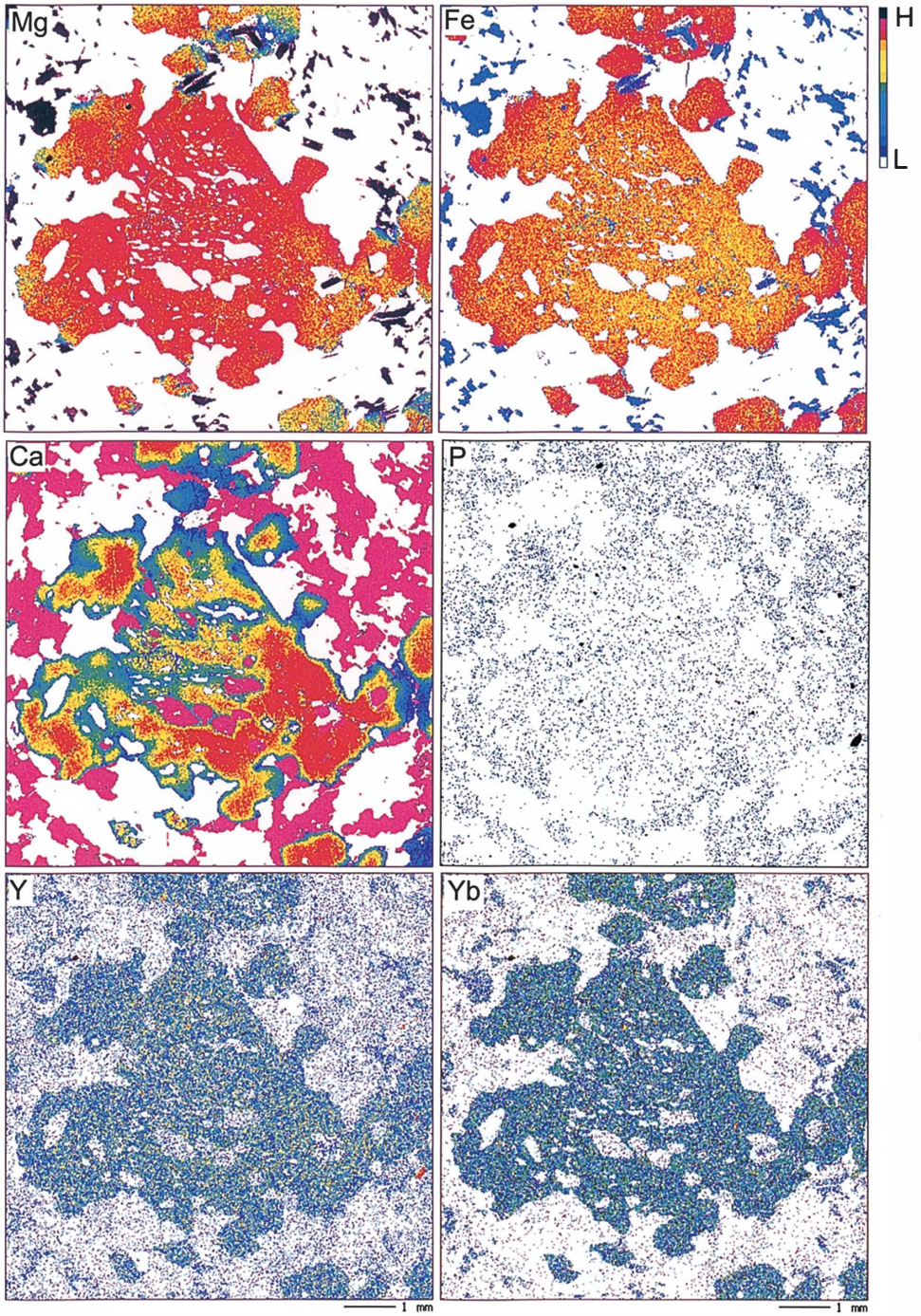

Fig. 15. Color X-ray intensity map of garnet in melanocratic garnet-biotite gneiss (Sample: 99020306-M).

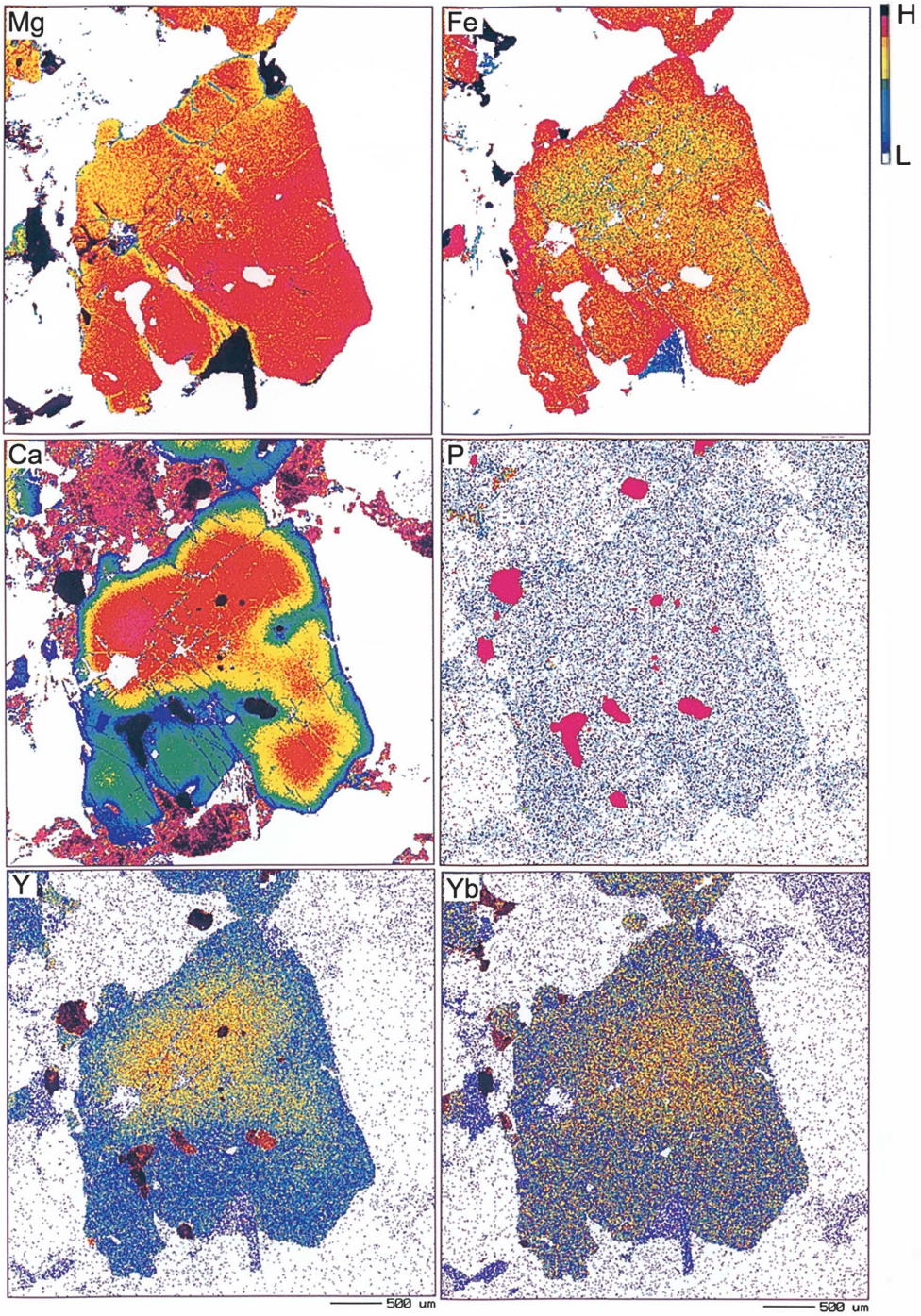

Fig. 16. Color X-ray intensity map of garnet in leucocratic garnet-biotite gneiss (Sample: 99020501).

contents decreasing from core to rim, and MgO increasing from core to rim. The zoning patterns are nearly concentric and symmetric in garnet-sillimanite and garnet-spinel-sillimanite gneiss (Fig. 12 and 13), although garnet from garnet-biotite gneiss shows asymmetric zoning (Figs. 14–16). The Y and Yb contents of garnet from garnet-sillimanite gneisses decrease toward rims. In contrast, the P content of garnet increases towards rims (Fig. 12). In garnet-spinel-sillimanite gneiss, P and Yb contents of garnet are not zoned. At the edges of garnet grains, there is an increase of Y content (Fig. 13). The Y and Yb contents of garnet from the boundary between leucosome and melanosome in melanocratic garnet-biotite gneiss decrease toward rims. In contrast, the P content in garnet increases toward rims (Fig. 14). In the melanosome of the melanocratic garnet-biotite gneiss, Y and Yb zoning patterns of garnet are not clear, though P shows slight zoning and relatively higher concentration in rims (Fig. 15). The Y and Yb contents of garnet from leucocratic garnet-biotite gneiss decrease toward rims, but P zoning is not visible (Fig. 16).

4.2.2. Biotite

The X_{Mg} compositions of biotite range between 0.53 to 0.59 in garnet-spinel-sillimanite gneiss, 0.64 to 0.8 in melanocratic garnet-biotite gneiss, and 0.46 to 0.54 in leucocratic garnet-biotite gneiss (Fig. 17). The highest TiO_2 content occurs in garnet-biotite gneiss, where it reaches a maximum of about 6.3 wt%. The X_{Mg} value and TiO_2 content of biotite inclusions within garnet in garnet-biotite gneiss tend to be slightly higher (about 7 wt% TiO_2) than in the matrix.

Fluorine contents of melanocratic and leucocratic garnet-biotite gneiss are between 0.5–1.8 and 0.8–1.55 wt%, respectively (Fig. 18). In garnet-spinel-sillimanite gneiss, biotite contains up to 0.6 wt% F. Biotite or phlogopite formed under UHT conditions

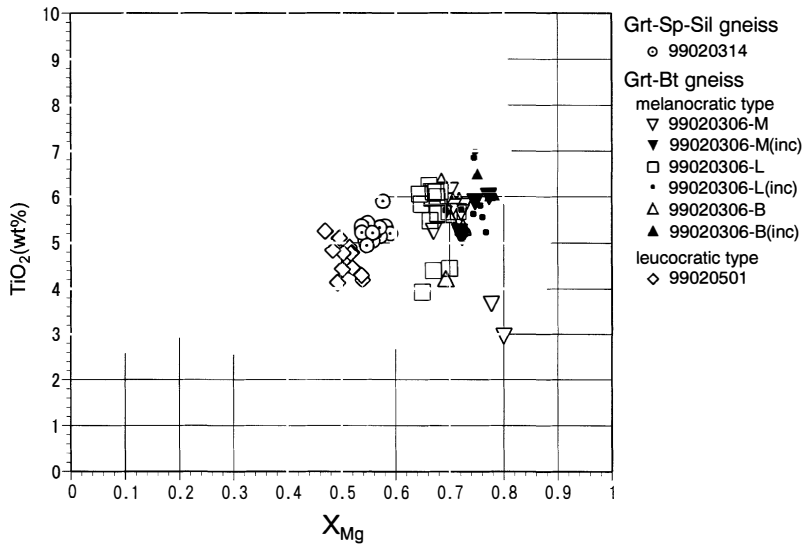

Fig. 17. Variation of TiO_2 and X_{Mg} in biotite in garnet-spinel-sillimanite gneiss and garnet-biotite gneiss.

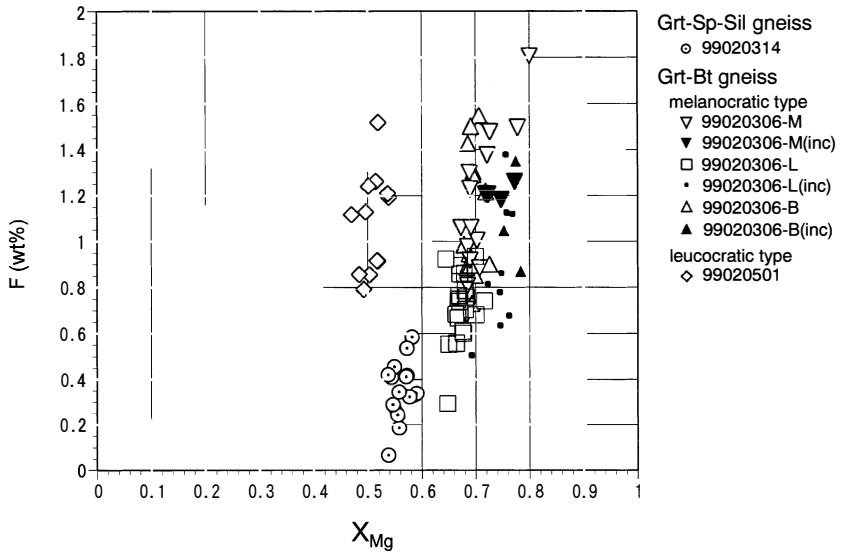

Fig. 18. Variation of F and X_{Mg} in biotite in garnet-spinel-sillimanite gneiss and garnet-biotite gneiss.

sometimes has fluorine contents up to 8 wt% (Motoyoshi, 1998). Biotite in garnet-biotite gneiss from Skallevikshalsen, however, has lower fluorine content compared with UHT metamorphic high-fluorine biotite.

4.2.3. Plagioclase

The An and Or contents of plagioclase are shown in Fig. 19. Anorthite (An) components of plagioclase are highest (An_{32-43}) in melanocratic garnet-biotite gneiss. Plagioclase compositions are about An_{28-32} in garnet-sillimanite gneiss and An_{30-32} in leucocratic garnet-biotite gneiss. In garnet-spinel-sillimanite gneiss, calcium content of plagioclase varies from An_{21} to An_{39}. The Or component of plagioclase has almost the same value for both rock types ($\sim Or_{0.7-3}$). Ca-contents of plagioclase inclusions within garnet in garnet-biotite gneiss and garnet-spinel-sillimanite gneiss tend to be distinctly higher than in the matrix. Plagioclase inclusions in garnet-biotite gneiss have higher K contents than in the matrix, whereas K contents in garnet-spinel-sillimanite gneiss have the same Or value in inclusions and the matrix.

The An and P_2O_5 contents of plagioclase are shown in Fig. 20. The P_2O_5 contents of plagioclase in the matrix of all rocks types are similar. Plagioclase inclusions within garnet from garnet-spinel-sillimanite gneiss and melanocratic garnet-biotite gneiss show relatively lower P_2O_5 contents than in the matrix.

4.2.4. K-feldspar

The Or component and BaO contents of K-feldspar are shown in Fig. 21. K-feldspar compositions have the widest variation in garnet-spinel-sillimanite gneiss (Or_{72-96}). The K_2O content of K-feldspar in garnet-sillimanite gneiss and leucocratic garnet-biotite gneiss are similar ($\sim Or_{84-94}$). Melanocratic garnet-biotite gneiss has K-feldspar with compositions from Or_{82-96}. K-feldspar in garnet-spinel-sillimanite

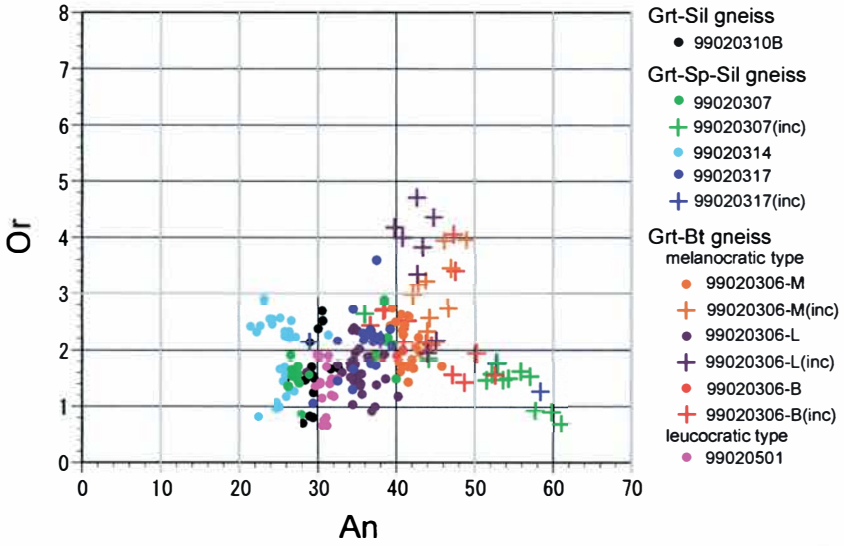

Fig. 19. Variation of Or and An content of plagioclase. 99020306-M: melanosome in melanocratic type. 99020306-L: leucosome in melanocratic type. 99020306-B: boundary between melanosome and leucosome in melanocratic type. (inc): inclusion composition.

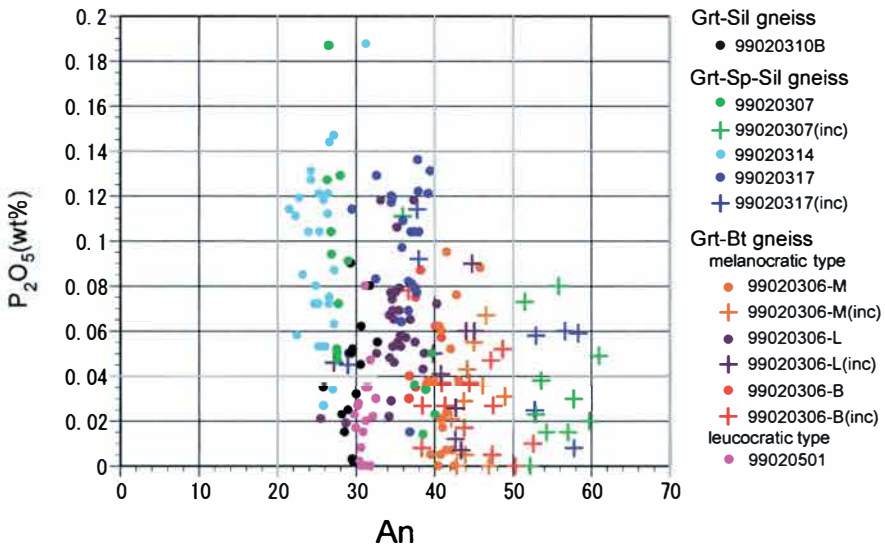

Fig. 20. Variation of P_2O_5 and An in plagioclase. 99020306-B: boundary between melanosome and leucosome in melanocratic type.

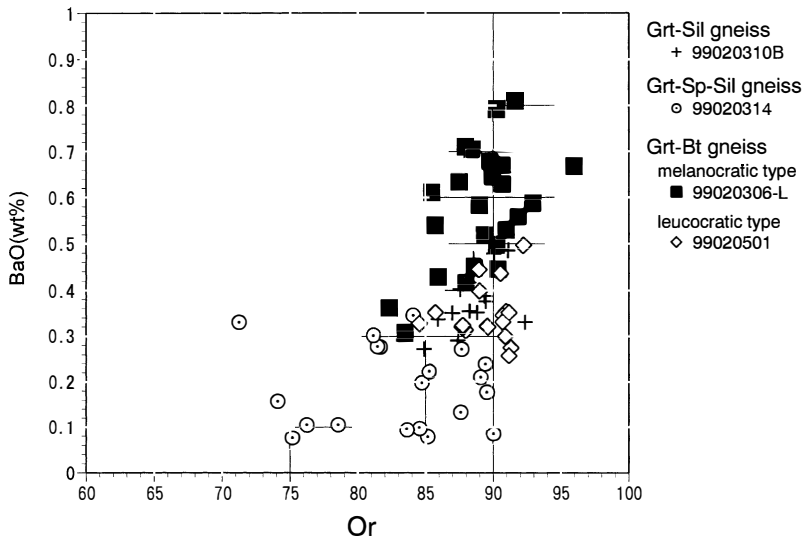

Fig. 21. Plot of BaO versus Or in K-feldspar.

gneiss has low BaO contents (0.1–0.35 wt%), whereas K-feldspar in melanocratic garnet-biotite gneiss has higher BaO (maximum 0.8 wt%). The BaO contents of K-feldspar in garnet-sillimanite gneiss and leucocratic garnet-felsic gneiss range from 0.26 to 0.5 wt%.

4.2.5. Pyroxenes

Pyroxenes are present only in mafic gneiss, where orthopyroxene coexists with clinopyroxene. Orthopyroxene grains are unzoned with X_{Mg} values and Al_2O_3 contents of around 0.4 and <1 wt%, respectively. In general, clinopyroxene shows compositional zoning, with X_{Mg} and wollastnite (Wo) content lowest in cores ($X_{Mg}=0.45$ and Wo_{31}) and increasing toward rims ($X_{Mg}=0.56$ and Wo_{47}).

4.2.6. Amphibole

Amphibole in mafic gneiss is ferropargasite following the classification of amphiboles by Leake *et al*. (1997). The amphibole has $X_{Mg}=0.41$–0.48 and Al_2O_3 and TiO_2 contents range between 11.5–12.3 wt% and 1.7–2.4 wt% respectively.

4.2.7. Spinel

Spinel from garnet-spinel-sillimanite gneiss has Cr_2O_3 and ZnO contents of 0.1 to 0.4 wt% and 0.1 to 0.2 wt%, respectively. The spinels are mostly of hercynite composition $X_{Fe}=0.72$–0.82 where $X_{Fe}=Fe/(Fe+Mg+Zn)$.

5. Discussion

5.1. Metamorphic conditions

The high-grade metamorphic rocks in Skallevikshalsen are interpreted to represent various lithofacies. The anhydrous lithofacies occurring in this region, such as garnet-sillimanite gneiss and garnet-spinel-sillimanite gneiss lack hydrous minerals, suggesting

high temperature conditions during metamorphism. However, these lithologies contain no adequate mineral assemblages in order to estimate temperature and pressure conditions by geothermobarometry. Therefore, in this study, the pressure-temperature (*P-T*) conditions of metamorphism were estimated for garnet-biotite gneiss and mafic gneiss, using various published geothermometers and geobarometers. The geothermometers employed in this study are based on garnet-biotite Fe-Mg exchange equilibria (Ganguly and Saxena, 1984; Indares and Martignole, 1985; Dasgupta *et al.*, 1991), garnet-orthopyroxene Fe-Mg exchange equilibria (Sen and Battacharya, 1984; Lee and Ganguly, 1988) and garnet-clinopyroxene Fe-Mg exchange equilibria (Ellis and Green, 1979; Krogh, 1988). The geobarometers used are based on garnet-sillimanite-plagioclase-quartz (Newton and Haselton, 1981; Ganguly and Saxena, 1984), garnet-orthopyroxene-plagioclase-quartz (Perkins and Chipera, 1985) and garnet-clinopyroxene-plagioclase-quartz assemblages (Newton and Perkins, 1982).

For zoned garnets from garnet-biotite gneiss and mafic gneiss, calculations were made using the compositions of the most Mg-rich domains. It is probable that compositional modifications have occurred as a result of volume diffusion and Fe-Mg exchange during cooling from peak temperatures. Minerals in which element diffusion is rapid, such as biotite (Spear, 1993), are particularly susceptible to compositional

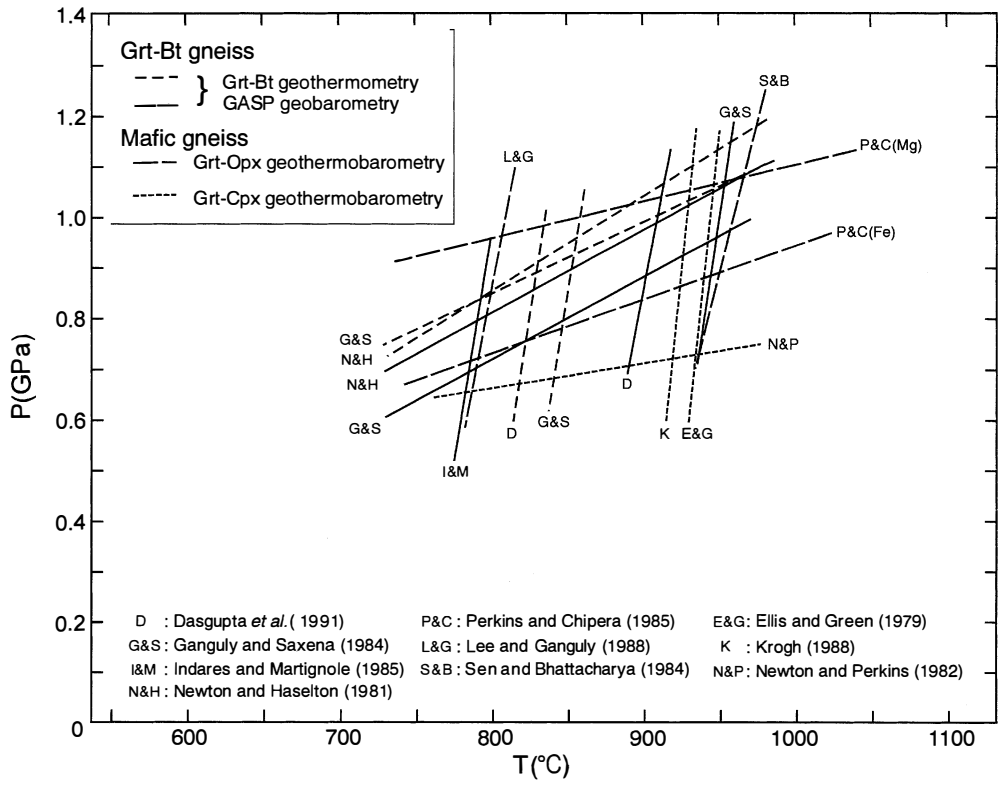

Fig. 22. P-T conditions of metamorphism estimated using geothermobarometry.

modification during retrograde cooling. Since Fe-Mg exchange can take place readily between biotite and adjacent garnet during cooling, temperature estimates were made using the compositions of biotite grains that are separated from garnet grains and that show the highest X_{Mg} values. In these cases, biotite and garnet may not be in equilibrium during peak metamorphism. However, the high Ti and relatively high F composition of biotite were probably acquired during high-temperature metamorphism. Moreover, biotite does not show retrograde reaction textures. It may be considered that biotite with high Ti, relatively high F content and the highest X_{Mg} values coexisted with Mg-rich garnet in near peak metamorphic conditions. The estimated temperature and pressure conditions are summarized in Fig. 22. *P-T* conditions estimated from assemblages in garnet-biotite gneiss range from 770 to 940°C and 0.65 to 1.2 GPa. Assemblages from mafic gneiss yield conditions of T = 780–960°C and P = 0.6–1.1 GPa. The metamorphic conditions estimated from the various lithofacies show good agreement. The metamorphic conditions estimated for Skallevikshalsen, when compared with those from previous studies (Fig. 23), lie between those estimated by Hiroi *et al*. (1987) for Prince Olav and Sôya Coasts, and Motoyoshi and Ishikawa (1997) for

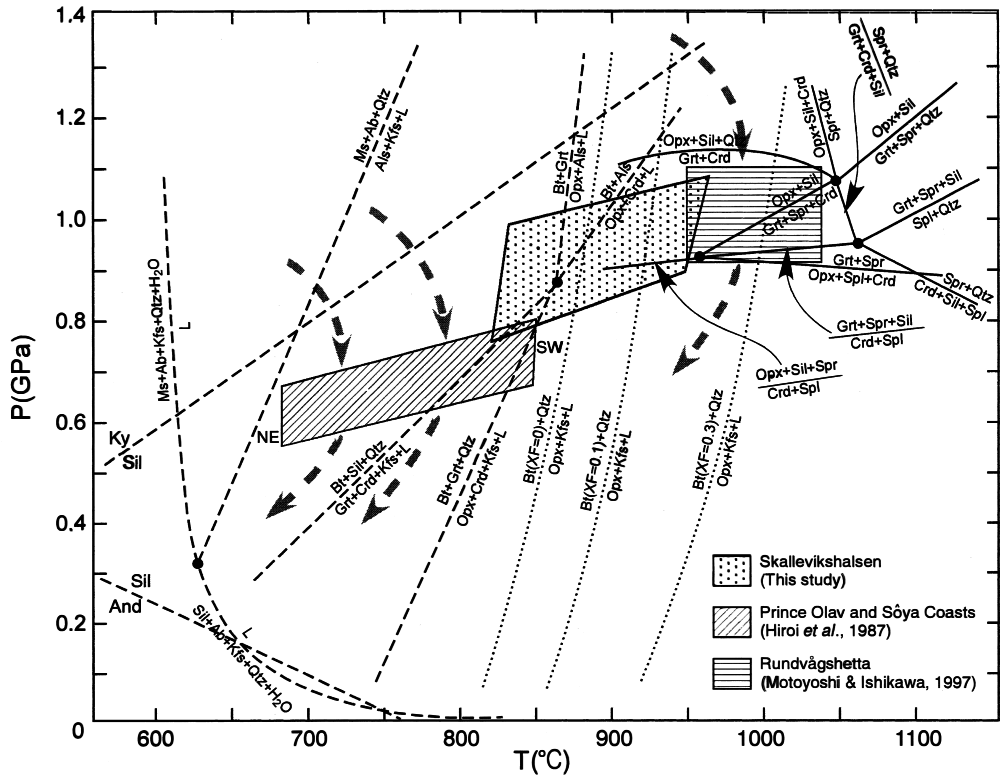

Fig. 23. P-T conditions in Skallevikshalsen. The reaction curves are modified from Spear et al. (1999: dashed lines) and Harley (1998: solid lines). Biotite melting reactions shown by dotted lines are those modified from Vielzeuf and Holloway (1988) and Hensen and Osanai (1994).

Rundvågshetta.

5.2. Possibility of partial melting

From the presence of leucosome, which occurs discordantly or semi-discodantly to the gneissose structure in garnet-biotite gneiss, it may be inferred that these rock types have undergone partial melting during high-temperature metamorphism. In Fig. 23, the relevant partial melting reaction curves in the pelitic system (after Vielzeuf and Holloway, 1988; Hensen and Osanai, 1994; Spear *et al*., 1999) are shown along with the metamorphic conditions of Skallevikshalsen and other parts of the Lützow-Holm Complex. The reaction representing partial melting involving biotite breakdown is as follows:

$$\text{biotite} + \text{quartz} = \text{orthopyroxene} + \text{K-feldspar} + \text{melt}. \quad (1)$$

This reaction is displaced towards high temperatures with increasing F content in biotite. For reaction (1), the curves for $X_F=0$, $X_F=0.1$ and $X_F=0.3$ are depicted (Fig. 23). Under the pressure conditions estimated above, melting reactions for $X_F=0$, 0.1 and 0.3 may have taken place at around 830–850°C, 870–890°C and 980–1020°C, respectively. It is inferred that in the case of Skallevikshalsen, metamorphic temperatures were high enough to cause the breakdown of fluorine-free biotite and consequent partial melting. Orthopyroxene, however, is absent in garnet-sillimanite gneiss, garnet-sillimanite-spinel gneiss and garnet-biotite gneiss. Thus, reaction (1) does not seem to take place in these rocks. If biotite contained $X_F=0.3$, reaction (1) did not proceed under the estimated metamorphic conditions. Apart from reaction (1), the partial melting phenomenon can also proceed according to the following reaction:

$$\text{biotite} + \text{sillimanite} + \text{quartz} = \text{garnet} + \text{cordierite} + \text{K-feldspar} + \text{melt}. \quad (2)$$

There is a high probability that the temperature of the above reaction is lower than that of reaction (1), even if fluorine was contained in biotite. Consequently, the estimated conditions for Skallevikshalsen lie within a field where partial melting can take place for typical pelitic rocks.

In the melanocratic garnet-biotite gneiss, garnet porphyroblasts in the leucosome and in the boundary between leucosome and melanosome commonly show euhedral to subhedral and poikiloblastic textures with euhedral feldspar and quartz inclusions (Fig. 7b and c). Plagioclase inclusions within garnet have typically higher An compositions than those in the matrix. This feature is also described by Hiroi *et al*. (1995), who argued that euhedral plagioclase inclusions in garnet were good indicators of partial melting. Furthermore, these garnets have relatively high Y content. It is known that Y and heavy rare earth elements such as Yb are concentrated in garnets that coexist with melt (Rollinson, 1993). The Y and Yb contents of garnet from garnet-biotite gneiss are highest in cores, whereas the P_2O_5 content of garnet in the garnet-biotite gneiss is lowest in cores (Fig. 14). We suggest that garnet coexisted with the melt while the core grew, and Y was concentrated in garnet cores. It is inferred that P entered the melt during partial melting, and in solid phases when the melt crystallized during cooling because P is an incompatible element (Rollinson, 1993). BaO content of K-feldspar in leucosome within melanocratic garnet-biotite gneiss shows high values (maximum 0.8

wt%). Although Ba is generally an incompatible element, K-feldspar possibly coexisted with the melt at high temperatures, because Ba is compatible with the crystal structure of potassium feldspar at high temperatures (Rollinson, 1993). The formation of garnet with poikiloblasts takes place during the prograde stage because the garnet grains have lower MgO in the cores than the rims. In such instances, partial melting in the leucosome and the margin proceeded according to the incongruent melting reaction proposed Hiroi *et al*. (1995):

$$\text{biotite} + \text{sillimanite} + \text{sodic plagioclase} + \text{K-feldspar} + \text{quartz} \pm H_2O = \text{garnet} + \text{calcic plagioclase} + \text{melt}. \quad (3)$$

Garnet grains with anhedral and concave morphology and that are characterized by domains with abundant inclusions occur in the melanosome of melanocratic garnet-biotite gneiss (Fig. 7a). This texture suggests resorption because the concave grain edges truncate dusty cores and is clear margins. An contents of plagioclase inclusions within garnet in melanosome also tend to be distinctly higher than in the matrix. This garnet has relatively high Y and P contents, but lower than garnet in the leucosome. In the melanosome within melanocratic garnet-biotite gneiss, garnet presumably became unstable by the injection of melt or due to the back reaction of (3). The salient features of garnet in melanocratic garnet-biotite gneiss are shown in Fig. 24. Melanosome and leucosome have features typical of restitic lithofacies and melt products, respectively. The Y_2O_3 content of garnet in leucocratic garnet-biotite gneiss is highest amongst the rock types. The content of P_2O_5 of garnet, however, is almost the same as that of other lithofacies. It is considered that the P content in the garnet is relatively low since apatite is a common constituent of this rock type. The BaO content of K-feldspar shows relatively high concentrations. Therefore, it is inferred that this lithofacies has also undergone partial melting during high-temperature metamorphism.

There are no migmatite structures in garnet-sillimanite gneiss. However, garnet in garnet-sillimanite gneiss has high Y and P_2O_5 contents and obvious zoning patterns similar to that in melanocratic garnet-biotite gneiss. Garnet shows the highest Y content in cores. By contrast, the P content of garnet in the garnet-sillimanite gneiss is lowest in cores. The compositional zoning of Y and P exhibited by garnet grains indicates that a marked change in the trace element distribution coefficient occurred during the evolution of this rock. The BaO content of K-feldspar also shows relatively high levels. We interpret this feature as a strong evidence for partial melting in the garnet-sillimanite gneiss, despite the absence of pronounced migmatitic structures. This lithofacies is presumably the restite, and the anhydrous nature resulted from the separation and segregation of a melt phase. Trace element behaviour in minerals is thus a powerful tool in determining the products of partial melting.

The garnet-spinel-sillimanite gneiss is also devoid of migmatitic structure. Although plagioclase inclusions within garnet in garnet-spinel-sillimanite gneiss have distinctly higher An content than in the matrix, evidence of partial melting is not recognized in garnet and K-feldspar. However, the crystallization of spinel has been confirmed experimentally to have resulted through disequilibrum melting (Beppu *et al*., 2002). Further detailed studies are required to evaluate the partial melting process in this lithofacies.

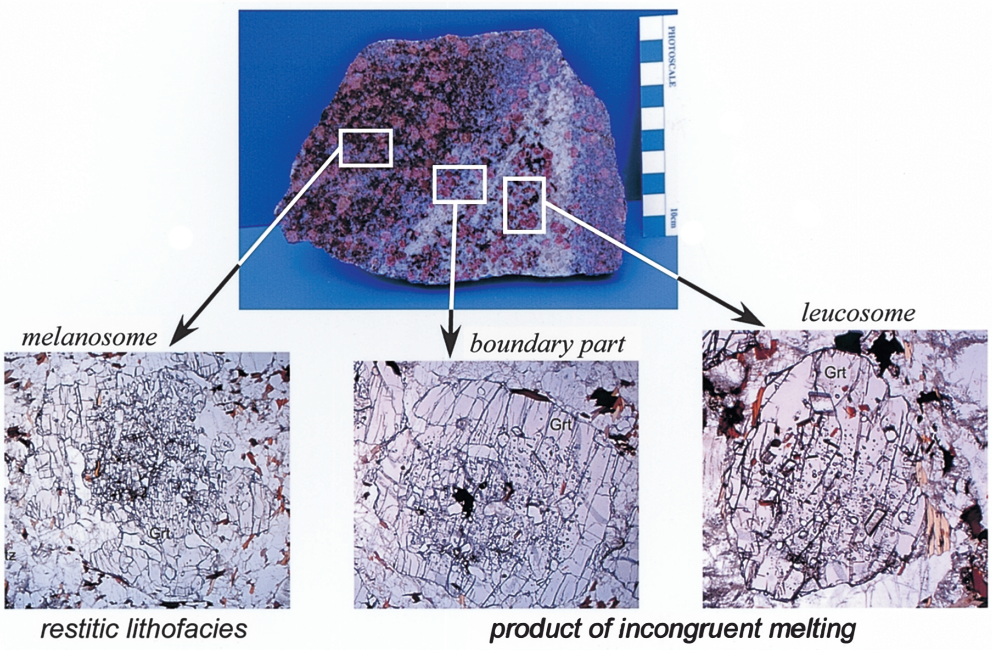

Fig. 24. Summary of salient features of melanocratic garnet-biotite gneiss. Melanosome features: relatively high Y and P contents for garnet and resorptional texture of garnet; matrix plagioclase compositions are relatively higher An values than the matrix. Therefore, it is inferred that melanosome is restitic lithofacies.
Boundary and leucosome features: euhedral feldspar and quartz inclusions in garnet; relatively high Y and P contents for garnet; plagioclase inclusions in garnet show higher An values than the matrix. Therefore, it is suggested that this domain is product of incongruent melting.

6. Conclusions

The metamorphic conditions for Skallevikshalsen were estimated to be 770–940°C and 0.65–1.2 GPa for garnet-biotite gneiss and 780–960°C and 0.6–1.1 GPa for mafic gneiss using various geothermometers and geobarometers. The *P-T* conditions for Skallevikshalsen lie well within a field where partial melting can take place in typical pelitic rocks.

Assessment of the occurrence of partial melting was performed using indicators such as garnet poikiloblastic texture with euhedral feldspar and quartz inclusions, plagioclase composition, Y and P contents of garnet and BaO content of K-feldspar. Garnet-biotite gneiss has well-developed migmatitic structure. Therefore, garnet-biotite gneiss has undergone partial melting during high-temperature metamorphism. In melanocratic garnet-biotite gneiss, leucosome and boundaries between leucosome and melanosome are melt products, whereas melanosome is restitic. Garnet in garnet-sillimanite gneiss has high Y and P_2O_5 contents and shows chemical zoning. Garnet-sillimanite gneiss is likely to be the restitic product of partial melting, despite the absence

of pronounced migmatitic structures. The integration of texture and trace element behaviour in minerals is a good indicator of partial melting.

Acknowledgments

We would like to sincerely thank all members of JARE-40, and all crew members of the icebreaker *Shirase*. Thanks are also due to Prof. Y. Osanai, Dr. M. Owada and Dr. T. Kawakami for their helpful discussions. The author also would like to thank Prof. M. Santosh at Kochi University for helpful discussions and for critical reading of the manuscript. Drs. T. Ikeda and N. Kelly are thanked for constructive reviews.

Reference

Beppu, M., Furukawa, N. and Hiroi, Y. (2002): Spinel-producing partial melting reaction in pelitic gneisses: petrographical and synthetic experimental approach. Jpn. Mag. Mineral. Petrol. Sci., **31**, 2, 97–110.

Dasgupta, S., Sengupta, P., Guha, D. and Fukuoka, M. (1991): A refined garnet-biotite Fe-Mg exchange geothermometer and its application in amphibolites and granulites. Contrib. Mineral. Petrol., **109**, 130–137.

Ellis, D.J. and Green, D.H. (1979): An experimental study of the effect of Ca upon garnet-clinopyroxene Fe-Mg exchange equilibria. Contrib. Mineral. Petrol., **71**, 13–22.

Fraser, G., McDougall, I., Ellis, D.J. and Williams, I.S. (2000): Timing and rate of isothermal decompression in Pan-African granulites from Rundvågshetta, East Antarctica. J. Metamorph. Geol., **18**, 441–454.

Ganguly, J. and Saxena, S. (1984): Mixing properties of aluminosilicate garnets: constraints from natural and experimental data, and applications to gerothermo-barometry. Am. Mineral., **69**, 88–97.

Harley, S.L. (1998): On the occurrence and characterization of ultrahigh-temperature (UHT) crustal metamorphism. Geol. Soc. London, Spec. Publ., **138**, 75–101.

Hensen, B.J. and Osanai, Y. (1994): Experimental study of dehydration melting of F-biotite in model pelitic compositions. Mineral. Mag., **58A**, 410–411.

Hiroi, Y., Shiraishi, K., Yanai, K. and Kizaki, K. (1983): Aluminum silicates in the Prince Olav and Sôya Coasts, East Antarctica. Mem. Natl Inst. Polar Res., Spec. Issue, **28**, 115–131.

Hiroi, Y., Shiraishi, K., Motoyoshi, Y., Kanisawa, S., Yanai, K. and Kizaki, K. (1986): Mode of occurrence, bulk chemical compositions, and mineral textures of ultramafic rocks in the Lützow-Holm Complex, East Antarctica. Mem. Natl Inst. Polar Res., Spec. Issue, **43**, 62–84.

Hiroi, Y., Shiraishi, K., Motoyoshi, Y. and Katsushima, T. (1987): Progressive metamorphism of calc-silicate rocks from the Prince Olav and Soya Coasts, East Antarctica. Proc. NIPR Symp. Antarct. Geosci., **1**, 73–97.

Hiroi, Y., Motoyoshi, Y., Shiraishi, K. and Ellis, D.J. (1995): The significance of euhedral calcic plagioclase inclusions in garnet from the Lützow-Holm Complex, East Antarctica: A textural indicator of partial melting in pelitic gneisses. Proc. NIPR Symp. Antarct. Geosci., **8**, 107–120.

Indares, A. and Martignole, J. (1985): Biotite-garnet geothermometry in the granulite facies: the influence of Ti and Al in biotite. Am. Mineral., **70**, 272–278.

Krogh, E.J. (1988): The garnet-clinopyroxene Fe-Mg geothermometer-a reinterpretation of existing experimental data. Contrib. Mineral. Petrol., **99**, 44–48.

Leake, B.E., Woolley, A.R., Arps, C.E.S., Brich, W.D., Gilbert, M.C. *et al*. (1997): Nomenclature of amphiboles: Report of the Subcommittee on Amphiboles of the International Mineralogical Association, Commission on New Minerals and Mineral Names. Am. Mineral., **82**, 1019–1037.

Lee, H.Y. and Ganguly, J. (1988): Equilibrium compositions of coexisting garnet and orthopyroxene: Experimental determinations in the system FeO-MgO-Al_2O_3-SiO_2, and applications. J. Petrol., **29**, 93–113.

Matsueda, T., Motoyoshi, Y. and Matsumoto, Y. (1983): Mg-Al skarns of the Skallevikhalsen on the east coast of Lützow-Holm Bay, East Antarctica. Mem. Natl Inst. Polar Res., Spec. Issue, **28**, 166–182.

Motoyoshi, Y. (1986): Prograde and progressive metamorphism of the granulite-facies Lützow-Holm Bay region, East Antarctica. D. Sc. Thesis, Hokkaido Univ., 238 p.

Motoyoshi, Y. (1998): Ultra-high temperature metamorphism of the Napier Complex, East Antarctica: a metamorphic perspective. J. Geol. Soc. Jpn., **104**, 794–807 (in Japanese with English abstract).

Motoyoshi, Y. and Ishikawa, M. (1997): Metamorphic and structural evolution of granulites from Rundvågshetta, Lützow-Holm Bay, East Antarctica. The Antarctic Region: Geological Evolution and Processes, ed. by C.A. Ricci. Siena, Terra Antarct. Publ., 65–72.

Newton, R.C. and Haselton, H.T. (1981): Thermodynamics of the garnet-plagioclase-Al_2SiO_5-quartz geobarometer. Thermodynamics of Minerals and Melts, ed. by R.C. Newton *et al*. New York, Springer, 131–147.

Newton, R.C. and Perkins, D. (1982): Thermodynamic calibration of geobarometers based on the assemblage garnet-plagioclase-orthopyroxene (clinopyroxene)-quartz. Am. Mineral., **69**, 203–222.

Rollinson, H. (1993): Using Geochemical Data: Evaluation, Presentation, Interpretation. Longman, 352 p.

Perkins, D., III and Chipera, S.V. (1985): Garnet-orthopyroxene-plagioclase-quartz barometry: refinement and application to the English River subprovince and the Minnesota River valley. Contrib. Mineral. Petrol., **89**, 69–80.

Sen, S.K. and Bhattacharya, A. (1984): An orthopyroxene-garnet geothermometer and its application to the Madras charnockites. Contrib. Mineral. Petrol., **88**, 64–71.

Shiraishi, K., Hiroi, Y. and Motoyoshi, Y. (1989): Geological Map of Lützow-Holm Bay, Antarctica. Antarct. Geol. Map Ser., Sheet 12, Tokyo, Natl Inst. Polar Res.

Shiraishi, K., Hiroi, Y., Ellis, D.J., Fanning, M., Motoyoshi, Y. and Nakai, Y. (1992): The first report of a Cambrian orogenic belt in East Antarctica—An ion microprobe study of the Lützow-Holm Complex. Recent Progress in Antarctica Earth Science, ed. by Y. Yoshida *et al*. Tokyo, Terra Sci. Publ., 67–73.

Shiraishi, K., Ellis, D.J., Hiroi, Y., Fanning, C.M., Motoyoshi, Y. and Nakai, Y. (1994): Cambrian orogenic belt in East Antarctica and Sri Lanka: Implications for Gondwana assembly. J. Geol., **102**, 47–65.

Spear, F.S. (1993): Metamorphic Phase Equilibria and Pressure-Temperature-Time Paths. Washington, D.C., Mineral. Soc. Am., 799 p.

Spear, F.S., Kohn, M.J. and Cheney, J.T. (1999): P-T paths from anatectic pelites. Contrib. Mineral. Petrol., **134**, 17–32.

Vielzeuf, D. and Holloway, J.R. (1988): Experimental determination of the fluid absent melting relation in the pelieic system. Consequences for crustal differentiation. Contrib. Mineral. Petrol., **98**, 257–276.

Yoshida, M., Yoshida, Y., Ando, H., Ishikawa, T. and Tatsumi, T. (1976): Geological map of Skallen, Antarctica. Antarct. Geol. Map Ser., Sheet 9 (with explanatory text, 16p.), Tokyo, Natl Inst. Polar Res.